



Cite this: *Green Chem.*, 2025, **27**, 9313

## CO<sub>2</sub>-responsive membrane separation systems: a green solution for efficient separations†

Ling Lei,<sup>‡,a</sup> Haohao Liu,<sup>‡,a</sup> Yunxiang Bai,<sup>a</sup> Chunfang Zhang,<sup>a</sup> Mingjie Yin,<sup>ID, b</sup> Wentao Wang<sup>c</sup> and Liangliang Dong<sup>ID, \*a</sup>

Membrane separation technology, which is characterized by its green, environmentally friendly, efficient, and continuous operation, has become indispensable in modern separation processes. It has widespread applications in pharmaceuticals, mineral extraction, and water purification. Because efficient and stable separation processes often require the integration of components across isolated, functionally distinct regions and the synergistic achievement of separation outcomes, membrane systems have emerged as a prominent trend within the field of membrane separation. Among them, CO<sub>2</sub>-responsive materials are an important research hotspot because of their precise and efficient separation performance caused by their green driving mode, mild and green condition, non-accumulation, and excellent reversibility. This review comprehensively investigates the history of the development of CO<sub>2</sub>-responsive membrane separation systems, including their CO<sub>2</sub>-responsive mechanisms, fabrication methods, critical characterization techniques, and potential applications. The review culminates in a forward outlook, summarizing future research directions as well as highlighting challenges in CO<sub>2</sub>-responsive membrane separation systems and emerging potential applications.

Received 14th January 2025,

Accepted 27th June 2025

DOI: 10.1039/d5gc00220f

rsc.li/greenchem

### Green foundation

1. CO<sub>2</sub>-responsive membrane separation systems primarily consist of CO<sub>2</sub>-responsive membranes and draw solutions. CO<sub>2</sub>, an abundant and inexpensive earth resource, can be utilized as a stimulus to reversibly regulate material properties, including pore size, wettability, surface potential, and osmotic pressure, within CO<sub>2</sub>-responsive membrane separation systems to achieve highly efficient, precise, and intelligent separation.
2. This study systematically investigates the history of the development of CO<sub>2</sub>-responsive membrane separation systems, including their CO<sub>2</sub>-responsive mechanisms, fabrication methods, critical characterization techniques, and potential applications.
3. Despite the existing industrial demand for CO<sub>2</sub>-responsive membrane separation systems, challenges persist in scaling up CO<sub>2</sub>-responsive material production and developing sophisticated control systems to ensure stable and reliable system operations.

## 1. Introduction

In nature, stimulus-responsive cell membranes regulate energy transfer and molecular exchange in response to external stimuli, representing one of the most efficient biological processes.<sup>1–3</sup> To mimic and better understand these responsive functions, an increasing number of artificial stimulus-respon-

sive membrane systems have been developed.<sup>4,5</sup> The responsiveness of such systems is primarily achieved by integrating stimuli-responsive materials into traditional porous membranes or solutions, thereby enhancing their functionality and performance beyond the limitations of conventional technologies. Upon exposure to external stimuli, including heat,<sup>6,7</sup> pH,<sup>8,9</sup> light,<sup>10,11</sup> magnetic fields,<sup>12,13</sup> or electrical current,<sup>14,15</sup> these materials within a membrane system can exhibit structural, morphological, or molecular conformational alterations, thereby modulating pore sizes and surface properties to regulate permeability and separation selectivity. However, the use of these stimuli often faces economic, environmental, and by-product pollution concerns.<sup>4,5,16</sup> Therefore, the development of novel stimulus-responsive methods triggered by environmentally friendly and cost-effective stimuli is crucial.

Compared with other stimuli, CO<sub>2</sub> is environmentally benign, does not lead to chemical species accumulation, and

<sup>a</sup>Key Laboratory of Synthetic and Biological Colloids, Ministry of Education, School of Chemical and Material Engineering, Jiangnan University, Wuxi 214122, China.  
E-mail: liangliangdong@jiangnan.edu.cn

<sup>b</sup>Beijing Key Laboratory for Green Catalysis and Separation, Department of Chemical Engineering, Beijing University of Technology, Beijing 100124, China

<sup>c</sup>School of Materials Science and Engineering, Zhejiang Sci-Tech University, Hangzhou 310018, China

† Electronic supplementary information (ESI) available. See DOI: <https://doi.org/10.1039/d5gc00220f>

‡ These authors contributed equally to the work.

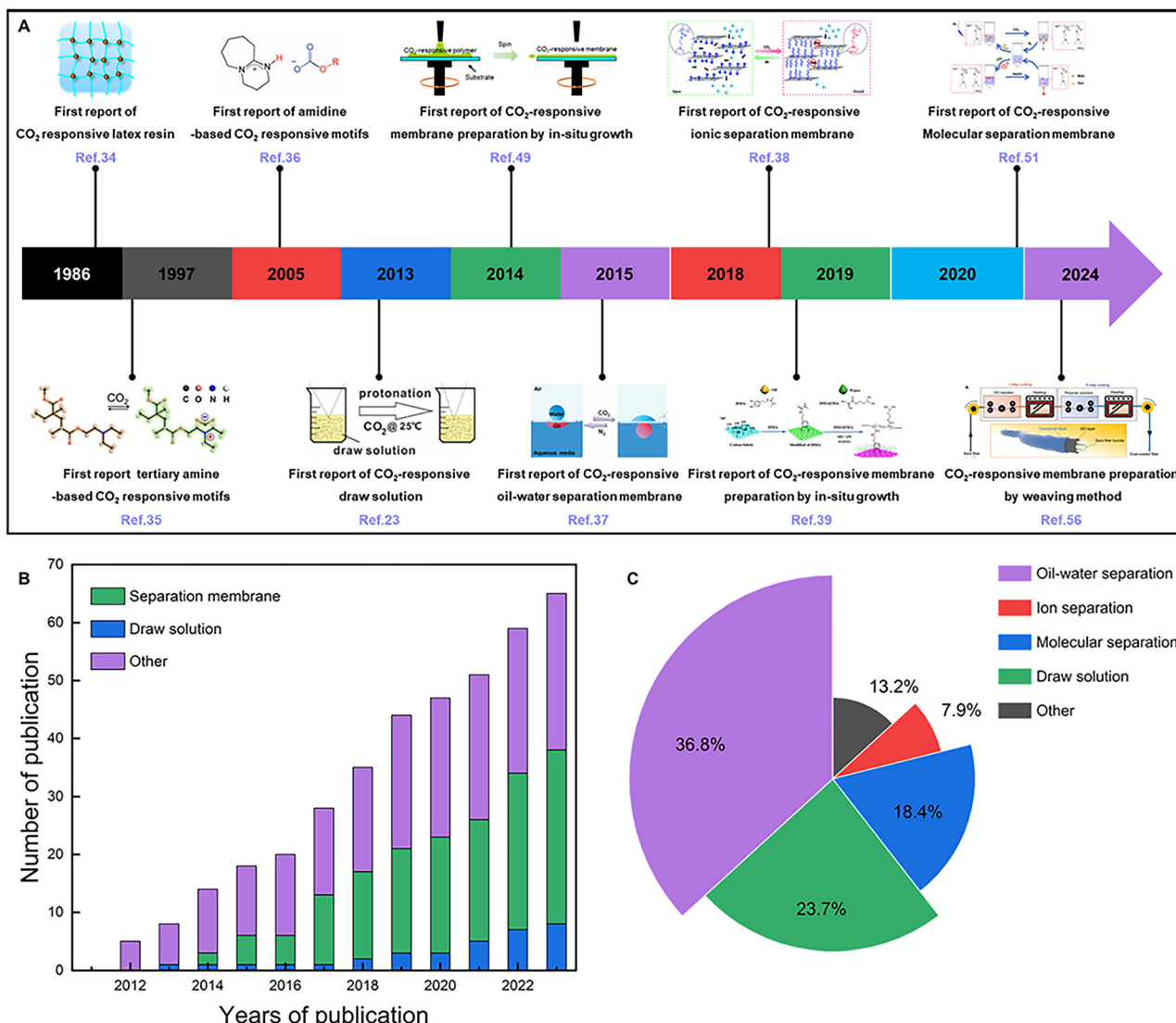


**Fig. 1** CO<sub>2</sub>-responsive materials for membrane separation systems. (A) Timeline of milestones for CO<sub>2</sub>-responsive materials in a membrane system. (B) Increasing scientific interest in CO<sub>2</sub>-responsive materials within membrane systems. (C) Research related to CO<sub>2</sub>-responsive membrane systems, reflecting potential fields of application.<sup>34,39</sup>



Ling Lei

Ling Lei received her Bachelor's degree in materials chemistry from Zhoukou Normal University, China, in 2023. She is currently a graduate student under the supervision of Prof. Liangliang Dong at Jiangnan University. Her research focuses on the design of CO<sub>2</sub>-responsive draw solutions and the investigation of membrane performance in forward osmosis (FO).



Haohao Liu

Haohao Liu received his BSc degree in textile engineering at Yancheng Institute of Technology, China, in 2018. He is currently a PhD candidate under the supervision of Prof. Liangliang Dong at Jiangnan University. His research focuses on the design and synthesis of three dimensional covalent organic frameworks for antibiotic desalination.

can be readily introduced into or removed from a system, making it a well-suited stimulus source for responsive membrane systems.<sup>17–21</sup> The implementation of such responsive membrane systems often requires integrating CO<sub>2</sub>-responsive polymers into critical components, such as the membrane material<sup>16</sup> and draw solution.<sup>22–27</sup> When employed in membrane materials, CO<sub>2</sub> treatment can reversibly modulate the pore size, surface potential, and wettability,<sup>28–32</sup> enabling the separation of components with distinct characteristics and sizes (Table S1†). In draw solutions for forward osmosis (FO), CO<sub>2</sub> treatment can reversibly adjust osmotic pressure, providing a strong driving force for system operation.<sup>25,27,33</sup> This transmembrane driving force, based on thermodynamically spontaneous processes, results in an energy consumption of 50% lower than that of conventional pressure-driven membranes (Table S2†).

Fig. 1A and B present a historical timeline highlighting key milestones and the exponential increase in related publications as valid supporting evidence for this view. In addition to the development of CO<sub>2</sub>-responsive motifs, fabrication methods are considered key drivers for the rapid development of CO<sub>2</sub>-responsive polymers within membrane systems.<sup>40</sup> These methods not only affect the physicochemical properties and separation performance of the membranes, but also directly determine their industrial application potential (such as cost, operational stability, reproducibility, and process design). To date, various CO<sub>2</sub>-responsive polymers have been synthesized using techniques such as free radical polymerization (FRP) and atom transfer radical polymerization (ATRP)<sup>41–43</sup> and subsequently fabricated into film-forming products *via* methods such as spin coating, doctor blading, *in situ*

growth, electrospinning, and weaving.<sup>44–52,54–56</sup> These materials have found widespread applications in oil–water separation, desalination, protein molecular separation, and CO<sub>2</sub>-responsive draw solutions (Fig. 1C).<sup>17</sup>

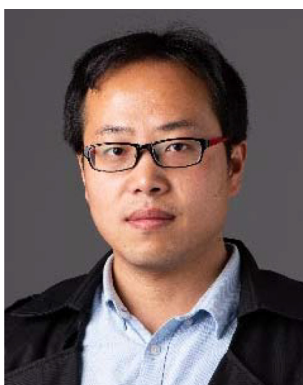
Given the numerous advantages of CO<sub>2</sub> over other stimuli, research on CO<sub>2</sub>-responsive membrane systems has accelerated significantly in recent years (Table S3†). However, a comprehensive review that systematically summarizes these materials is currently lacking. This review aims to comprehensively address this gap by focusing on the material development, preparation technology, characterization methods, and application attempts of CO<sub>2</sub>-responsive membrane separation systems. Finally, we conclude by outlining the current challenges and future perspectives to accelerate the practical application of CO<sub>2</sub>-responsive membrane systems.

## 2. CO<sub>2</sub>-responsive membrane separation system

A CO<sub>2</sub>-responsive membrane separation system utilizes CO<sub>2</sub> as a stimulus to reversibly modulate the surface and the physicochemical properties of materials within the membrane system to ensure an efficient and precise separation process dominated by the CO<sub>2</sub> stimulus (Fig. 2). The CO<sub>2</sub>-responsive performance of a system depends on the synergistic interplay of three key components: CO<sub>2</sub>-responsive motifs, membrane materials, and draw solutions.

### 2.1. CO<sub>2</sub>-responsive motifs

**2.1.1. Tertiary amines.** Tertiary amines (–NR<sub>1</sub>R<sub>2</sub>) are typical CO<sub>2</sub>-responsive motifs that react not only with strong acids such as HCl but also with weak gaseous acids such as CO<sub>2</sub>.<sup>35</sup> The equilibrium constant ( $K_t$ ) for the reaction between a tertiary amine and CO<sub>2</sub> gas ranges from 1.3 to 45, indicating a reversible equilibrium.<sup>20</sup> The pK<sub>a</sub> value, which represents the logarithmic form of  $K_t$ , is a crucial parameter for evaluating the reversibility of CO<sub>2</sub>-responsive motifs. Lower pK<sub>a</sub> values indicate a greater propensity for deprotonation.<sup>16</sup> Owing to their relatively low pK<sub>a</sub> values, tertiary amines can be readily deprotonated through a simple procedure involving the bubbling of an inert gas, such as argon (Ar) or nitrogen (N<sub>2</sub>), through the aqueous medium. Therefore, when tertiary amine groups are incorporated into the polymer chain structure, alternating exposure to CO<sub>2</sub> and inert gases can complete the protonation and deprotonation of tertiary amines in a short time cycle, eliminating the need for energy-intensive heating procedures. This low-cost and gentle approach is reversible in terms of both the surface properties and the molecular conformation of the polymer, making tertiary amine-based polymers particularly attractive for CO<sub>2</sub>-responsive membrane systems. Tertiary amines are commercially available and inexpensive. However, the easy deprotonation process makes the tertiary amine unavailable at high temperatures unless the CO<sub>2</sub> pressure is significantly increased.<sup>57,58</sup>



Liangliang Dong

Dr Liangliang Dong received his BS degree (2010), MS degree (2013), and Ph.D. (2018) from Jiangnan University. In 2016, he attended the University of Sherbrooke in Canada for joint doctoral training under the supervision of Professor Yue Zhao and received a PhD from the University of Sherbrooke in 2018. He is currently a professor at the School of Chemistry and Materials Engineering at Jiangnan University, with

research interests in CO<sub>2</sub>-responsive membranes, gas separation membranes and nanofiltration membranes. He has acted as director of the 41st Chemical Industry and Engineering Society of China (CIESC), a member of the Youth Working Committee of the CIESC, and a member of the second session of the Daily Chemical Products Specialized Committee of the CIESC. He received the prestigious Young Scientist Award at the second International Congress on Separation and Purification Technology (ISPT 2024).

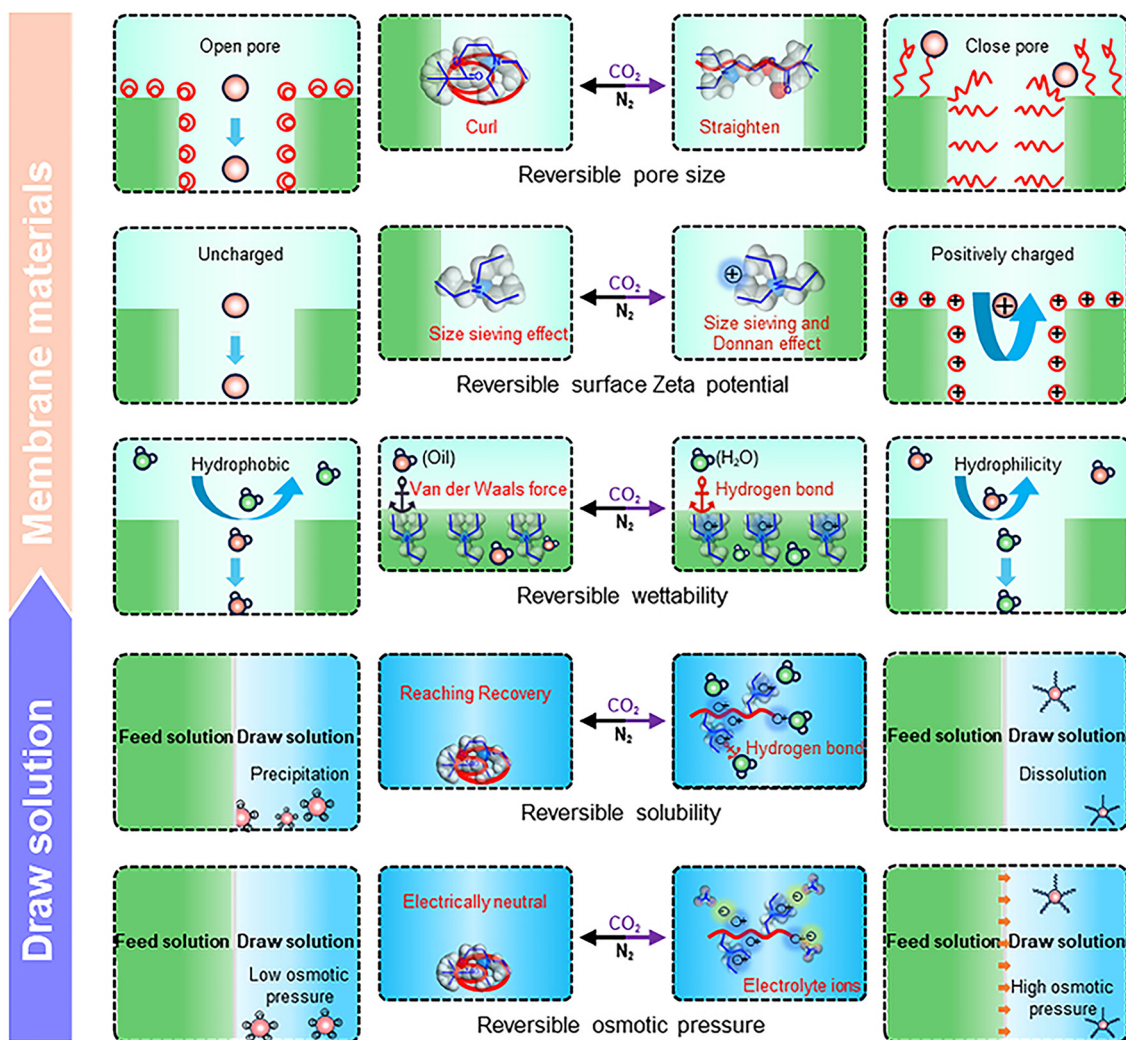


Fig. 2  $\text{CO}_2$ -responsive membrane separation systems mainly include membrane materials and draw solutions.

**2.1.2. Amidines.** Amidines, which are stronger bases than amines but weaker than guanidines and imidazoles,<sup>59,60</sup> undergo reversible protonation and deprotonation in aqueous solutions *via* the addition and removal of  $\text{CO}_2$ . Amidines containing N–R bonds may form carbamate salts in addition to, or instead of, bicarbonate salts. Consequently, amidines undergo a faster protonation process than tertiary amines, but their deprotonation requires more energy. This typically requires a thermal process instead of simply bubbling an inert gas such as argon (Ar) or nitrogen ( $\text{N}_2$ ) through an aqueous medium. The  $pK_a$  of amidines can be reduced by incorporating an aromatic substituent on either a nitrogen atom or a central carbon atom, resulting in amidines that exhibit  $\text{CO}_2$ -responsiveness more akin to tertiary amines. Owing to their  $\text{CO}_2$ -responsiveness, amidines have been utilized in the synthesis of  $\text{CO}_2$ -responsive amidine-containing (co)polymers. However, a significant challenge arises from the inherent susceptibility of amidines to hydrolysis in the absence of  $\text{CO}_2$ , which can potentially disrupt polymer self-assembly behavior. Moreover, the facile hydrolysis

of amidine groups necessitates stringent anhydrous and anaerobic conditions during synthesis, which significantly hinders large-scale production and practical applications.<sup>61,62</sup>

**2.1.3. Guanidines.** Guanidines are amine derivatives featuring a carbon atom bearing three nitrogen functional groups: one imine and two amine groups.<sup>36,63</sup> Structurally, they resemble amidines, which contain a carbon atom bonded to one imine and one amine. Because of the resonance stabilization of their conjugate acids, they are classified as organic superbases, particularly alkyl-substituted guanidine derivatives.<sup>64</sup> The high  $pK_a$  of guanidines (approximately 13.5) necessitates the use of energy-intensive processes, such as elevated temperatures and extended durations, to convert their bicarbonate salts to the neutral form. This limitation has hindered the development of membrane separation applications that involve temperature-sensitive components or large-scale operations. Consequently, a few reported instances of guanidine utilization exist in  $\text{CO}_2$ -responsive membrane systems (denoted by an asterisk (\*) in Table 1).<sup>65–67</sup>

**Table 1** Examples of CO<sub>2</sub>-responsive materials with different preparation methods, structures, and applications

Table 1 (Contd.)

Functionalities (R)	pK <sub>a</sub> values	Polymerization method	Chemical structure	Application	Ref.
	13.5	a		*	66
Guanidines		d		P(CPAM-co-AME)	67
	9.0	b			53
Amidines		e		PEO-b-PAD	59
	10-14.5	f		Acid amidine	69
Imidazoles		a		Alkyl imidazole	71
				I-PT	

Polymerization methods a, b, c, d, e, and f represent FTR, ATRP, RAFT, condensation, amide acetal formation, and alkylation, respectively. \* indicates that the material is not currently used in CO<sub>2</sub> responsive membrane separation systems.

While rapid deprotonation of guanidine typically requires elevated temperatures, this characteristic can be advantageous for applications operating in high-temperature environments. For instance, this property presents a significant opportunity for the development of CO<sub>2</sub>-responsive draw solutions. This advantage stems from the stable protonation process of guanidine-based draw solutions, which ensures high osmotic pressures for an extended period of time within a forward osmosis (FO) system.

**2.1.4. Imidazoles.** Imidazole is a five-membered aromatic heterocycle that contains two nitrogen atoms at positions 1 and 3. It possesses a planar structure with delocalized  $\pi$ -electrons which contribute to its aromatic character.<sup>68-71</sup> The presence of two ring nitrogen atoms significantly influences the chemical reactivity and biological properties, such as CO<sub>2</sub> responsiveness. When CO<sub>2</sub> is added to an aqueous solution, imidazole is protonated and converted to an imidazolium salt. However, like guanidines, imidazole exhibits high basicity, with pK<sub>a</sub> values ranging from 10 to 14.5, depending on the substituent groups. This high basicity renders deprotonation challenging and often requires elevated temperatures. Consequently, limited examples of imidazole-based polymers in membrane systems have been reported in the literature (Table 1).

## 2.2. CO<sub>2</sub>-responsive separation membranes

CO<sub>2</sub>-responsive separation membranes are one of the key components of a membrane system. To date, various techniques

have been employed to fabricate CO<sub>2</sub>-responsive separation membranes. In this section, we introduce and summarize the most commonly used methods for fabricating CO<sub>2</sub>-responsive separation membranes, such as spin coating, doctor blade, *in situ* growth, electropinning, and weaving methods (Fig. 3).

**2.2.1. Spin coating method.** Spin coating is a widely used technique for fabricating thin films in various fields including materials science, microelectronics, and optoelectronics. In this process, the substrate is affixed to a rotating disk and coated with a CO<sub>2</sub>-responsive polymer solution. The centrifugal force causes the spreading of the polymer solution, forming a structurally intact film on the substrate with the thickness controlled by the rotational speed and solution viscosity. Under conditions of constant polymer solution viscosity, increasing the rotational speed enables the fabrication of thin membranes with nanoscale thicknesses. However, excessively high speeds compromise the membrane-forming capability and induce nonuniform pore size distribution. Conversely, insufficient rotational speed tends to cause inhomogeneous membrane thickness, surface densification, and reduced porosity. Consequently, during membrane fabrication, the rotational speed must be precisely optimized within a specific range based on the rheological properties of the solution to ensure structural uniformity and controllable membrane thickness (Fig. 3A). In 2014, Wang *et al.* pioneered the use of spin-coating to fabricate a novel class of CO<sub>2</sub>-respon-

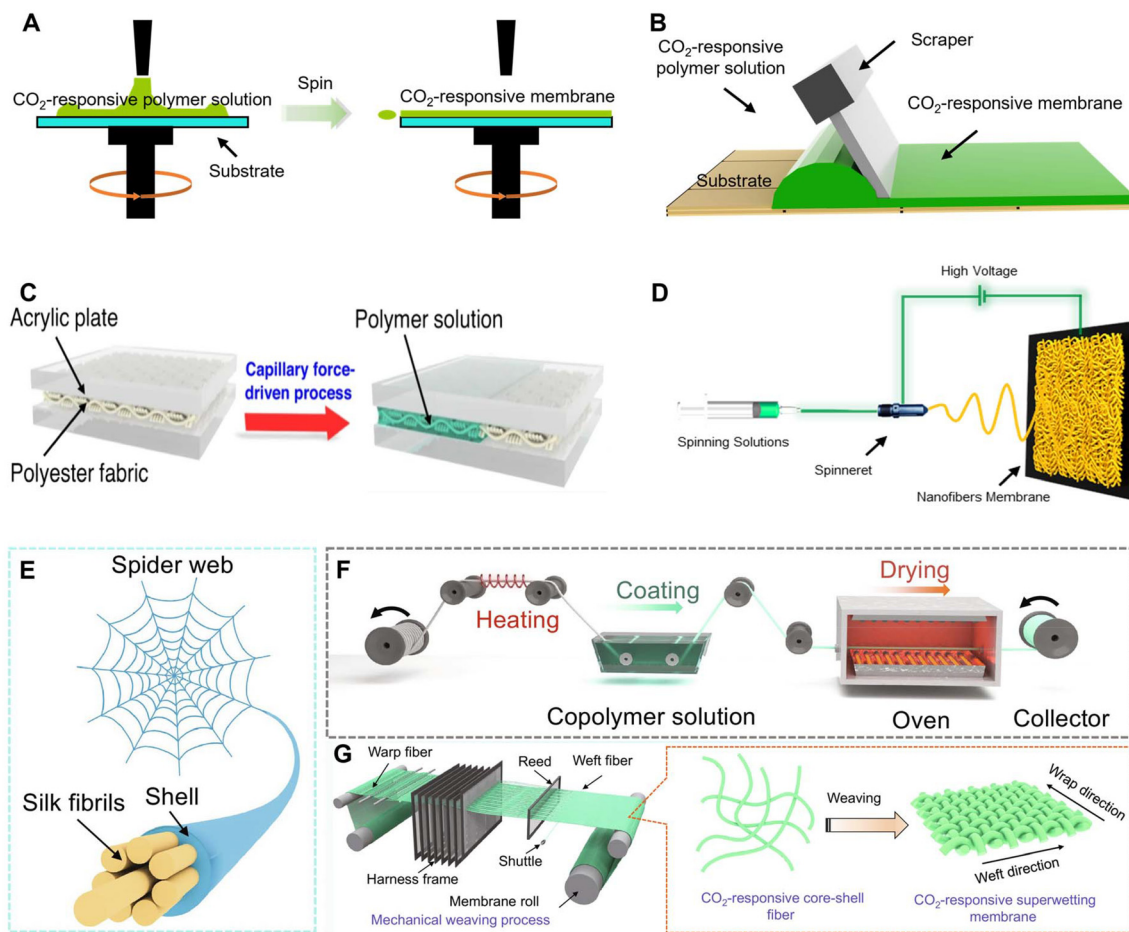


**Fig. 3** Preparation methods for  $\text{CO}_2$ -responsive separation membranes. (A) Spin coating method. (B) Doctor-blade method. (C) *In situ* growth method. Reprinted from ref. 49 copyright (2023) with permission from Springer Nature. (D) Electrospinning mode. (E–G) Weaving mode. Reprinted from ref. 55 copyright (2024) with permission from the American Association for the Advancement of Science (AAAS).

sive separation membranes. The entire preparation process involved spin-coating a chloroform solution of polystyrene-*b*-polyethylene oxide (PS-*b*-PEO) onto clean anodic aluminum oxide wafers at 1000 rpm for 30 seconds.<sup>47</sup> This resulted in smooth, defect-free PDMAEMA-*b*-PS membranes with thicknesses below 300 nm after the solvent removal. In the spin-coating method, smooth, flat inorganic substrates, such as silicon and anodized aluminum, facilitate the formation of uniform-thickness  $\text{CO}_2$ -responsive membranes. However, subsequent processes involving the separation of the membrane and substrate may compromise the quality of the  $\text{CO}_2$ -responsive membranes. In a follow-up study, Wang *et al.* utilized PDEAEMA-*b*-PS to fabricate  $\text{CO}_2$ -responsive membranes on PVDF substrates *via* spin coating.<sup>48</sup> The porous PVDF substrate, with its inherent ultrafiltration properties, served as a direct support for the 275 nm thick PDEAEMA-*b*-PS membrane, eliminating the need for membrane transfer. However, compared with the doctor blade method, the spin-coating method exhibits limitations in scalability owing to its reliance on specialized film-forming machinery, hindering its suitability for continuous, large-area  $\text{CO}_2$ -responsive membrane production.

**2.2.2. Doctor blade method.** The doctor blade method, a widely used industrial technique, enables continuous, controlled micron-thickness membrane production by adjusting parameters such as squeegee height and speed.<sup>45</sup> Precise regulation of the blade gap height enables accurate control over the membrane thickness, while optimization of the coating speed facilitates the fabrication of micro-scale separation membranes with uniform surface flatness and pore size distribution. At lower coating speeds, prolonged residence time of the polymer solution on the substrate promotes membrane thickening and concurrent failure in size-sieving performance. Conversely, excessively high coating speeds induce insufficient solution leveling, triggering surface ripples or structural defects alongside significant thickness reduction. Consequently, blade parameters must be precisely matched to the rheological properties of the solution to achieve controlled architecture of the membrane structures.  $\text{CO}_2$ -responsive separation membranes fabricated *via* the squeegee method involve the incorporation of  $\text{CO}_2$ -responsive agents into a film-forming polymerization solution. This mixture is uniformly coated onto the substrate using a squeegee (Fig. 3B). Guo *et al.*

synthesized a novel CO<sub>2</sub>-responsive copolymer, polyacrylonitrile-*co*-poly(2-diethylaminoethyl methacrylate) (PAN-*co*-PDEAEMA), using FRP. This copolymer was blended with PAN construction fluid and cast into membranes using the doctor-blade method.<sup>44</sup> A significant advantage of this method is its abilities to be easily laminated to existing industrial membranes, integrate CO<sub>2</sub>-responsive functionalities, and enable large-scale industrial applications. However, simple physical mixing between CO<sub>2</sub>-responsive agents and film-forming polymers usually results in an inhomogeneous and less robust distribution of responsive sites within the membrane, weakening the CO<sub>2</sub> responsiveness of membrane.<sup>46</sup> During the water phase transition process, the hydrophilic PDMAEMA and PDEAEMA segments dispersed on the outer surface membrane, while the hydrophobic PMMA segments intertwined with the equally hydrophobic PVDF inside the membrane, forming strong anchorage points. These structural features endow the PVDF-blended membrane with excellent CO<sub>2</sub> responsiveness and stability.

**2.2.3. *In situ* growth method.** *In situ* growth of films offers an alternative approach for the fabrication of CO<sub>2</sub>-responsive membranes. This method involves the *in situ* adsorption or assembly of CO<sub>2</sub>-responsive active substances onto a substrate membrane, which has the advantage of simplicity. Through precise regulation of substrate material composition, reaction time-temperature parameters during *in situ* growth, and solution concentration, thickness-tunable separation membranes ranging from nanometers to micrometers can be fabricated with pore sizes achieving sub-nanometer precision. Dong *et al.* employed a constrained self-assembly technique driven by capillary forces.<sup>49</sup> By confining a 10 wt% CO<sub>2</sub>-responsive polymer solution within a fabric membrane, with drying carried out under vacuum conditions at 50 °C for 24 h, they achieved a homogeneous coating both on the surface and within the fabric structure, synthesizing a separation membrane with a thickness of 150 µm and a pore size of approximately 0.1 µm (Fig. 3C). This approach offers a simple and scalable preparation process, enabling the production of large-area membranes (up to 3600 cm<sup>2</sup>) and demonstrating significant potential for large-scale industrial applications. However, it is widely believed that weak interfacial bonding between the active substance and substrate frequently compromises both the CO<sub>2</sub>-responsive membrane sensitivity to CO<sub>2</sub> and the cycling stability. Meng *et al.* addressed this limitation by developing a structurally stable cotton fabric grafted with p(DMA-DMAEMA).<sup>39</sup> Free-radical polymerization was employed to graft DMAEMA onto dopamine-modified cotton, resulting in strong interactions between dopamine and cotton and the formation of covalent bonds between dopamine and 2-(dimethylamino) ethyl methacrylate (DMAEMA). This enhanced interfacial bonding led to a fabric exhibiting stable and tunable oil-water wettability under alternating CO<sub>2</sub> and N<sub>2</sub> exposure. Importantly, the p(DMA-DMAEMA)-grafted cotton fabric maintained its reversible CO<sub>2</sub> response even after 500 abrasion cycles, which was attributed to the robust anchoring effect of the polydopamine layer.

**2.2.4. Electrospinning method.** Electrospinning is a versatile technique that employs a high-voltage electric field to

induce ejection of a polymer solution from a needle, resulting in the formation of nanofibers. These nanofibers subsequently self-assemble into nonwoven fabrics that can serve as promising membrane materials. By precisely controlling process parameters, such as voltage, solvent type, drum speed, and polymer viscosity, the morphology of the resulting nanofibers, including diameter, orientation, and surface roughness, can be meticulously tailored. Non-uniform electric field distribution and current fluctuations can lead to non-uniform membrane thicknesses. By increasing the electric field intensity, the fiber diameter is refined and the deposition rate per unit time is reduced, thereby decreasing the membrane thickness. By precisely adjusting parameters such as voltage, current density, and processing time, separation membranes with thicknesses ranging from several micrometers to hundreds of micrometers and sub-micron pore sizes can be fabricated (Fig. 3D). Owing to its simplicity and versatility, electrospinning has been widely adopted for fabricating CO<sub>2</sub>-responsive separation membranes. In 2015, Yuan *et al.* pioneered the development of CO<sub>2</sub>-responsive membranes *via* electrospinning. They synthesized polymethylmethacrylate-*co*-poly (N,N-dimethylaminoethyl methacrylate) (PMMA-*co*-PDEAEMA) CO<sub>2</sub>-responsive copolymers *via* free-radical polymerization and subsequently electrospun them into nanofibrous membranes with an average diameter of ~700 nm.<sup>37</sup> These membranes exhibited desirable properties, such as high porosity and a large surface-to-volume ratio, attributed to the interconnected fiber network, which facilitated enhanced CO<sub>2</sub>-responsive site exposure and improved response sensitivity.

In-depth research has led to the development of a diverse range of CO<sub>2</sub>-responsive electrospinning membranes, including those based on poly (pentafluorophenyl acrylate-*co*-4-acryloyloxy benzophenone) (P(PFPA-*co*-ABP))<sup>53</sup> and polyacrylonitrile-*co*-poly (N,N-diethylaminoethyl methacrylate) (PAN-*co*-PDEAEMA).<sup>52</sup> Furthermore, the incorporation of additional functionalized substances enabled the fabrication of multiresponsive membranes, enhancing their overall performance. For instance, to visualize wettability changes, Shirin-Abadi *et al.* incorporated hydroxyl-functionalized spirobifluorene (SPOH) into a poly (methyl methacrylate)-*co*-poly (N,N-diethylaminoethyl methacrylate) (PMMA-*co*-PDEAEMA) CO<sub>2</sub>-responsive polymer solution and subsequently fabricated a nonwoven film *via* electrospinning.<sup>51</sup> This innovative approach resulted in a membrane exhibiting CO<sub>2</sub>-triggered oil-water wettability switching, with the wettability change readily visualized by distinct color changes under UV light, attributed to the pronounced UV responsiveness of SPOH in weakly acidic environments.

**2.2.5. Weaving method.** Weaving, the process of the regular interlacing of warp and weft yarns on a loom, enables continuous, large-scale production of fabrics that can be considered microporous membranes. By optimising the controllable parameters such as fibre diameter, weaving density, and textural configuration, fibre membranes with a uniform thickness distribution, densely distributed membrane pores, and a narrow pore size distribution can be obtained. Refinement of

fiber diameter combined with increased weaving density effectively reduces pore size, while further adopting an appropriate textural patterning approach enables the fabrication of membranes with homogeneous pore structure and surface flatness. To mitigate yarn damage caused by repeated friction during the weaving process, sizing—the application of a polymer coating to yarns, typically employing polymers such as poly (polyvinyl alcohol) (PVA)—is an essential step (Fig. 3E).<sup>54</sup> Inspired by this technique, Dong *et al.* pioneered the development of CO<sub>2</sub>-responsive superwetting membranes (CO<sub>2</sub>-RSM) *via* the weaving method. This involved replacing the conventional PVA polymer solution with a CO<sub>2</sub>-responsive polymer solution (PMMA-*co*-PDEAEMA), successfully demonstrating the industrial-scale production of large-area CO<sub>2</sub>-RSM using established industrial coating and braiding equipment.<sup>55</sup> This method allows both controllable adjustment of the membrane aperture by programmed control of the density between the warp and weft yarns during the weaving process and easy preparation of a large-area CO<sub>2</sub>-RSM.

To address the critical challenges of low separation efficiency and high energy consumption stemming from the extended response times of conventional CO<sub>2</sub>-responsive separation membranes, Dong *et al.* prepared CO<sub>2</sub>-responsive superwetting membranes by mechanically weaving yarns with double-shell layers (*i.e.*, CO<sub>2</sub>-responsive PMMA-*co*-PDEAEMA polymer and photo-thermal-responsive GO layers).<sup>56</sup> Programmed knitting facilitated an ordered yarn arrangement and uniform graphene oxide (GO) distribution within the membrane. Leveraging the photothermal effect of the GO layer under near-infrared (NIR) irradiation, the deprotonation time of the CO<sub>2</sub>-responsive superwetting membranes varied from 20 min to 6 min. This resulted in a greater than two-fold enhancement in the oil–water wettability switching efficiency for the CO<sub>2</sub>-responsive superwetting membranes.

### 2.3. CO<sub>2</sub>-responsive draw solution

The draw solution provides the driving force in the forward osmosis process, which is a key factor in determining separation efficiency and accuracy. Compared with widely used inorganic salt-based drawing solutions,<sup>72,73</sup> CO<sub>2</sub>-responsive draw solutions have the potential to become the next generation of green and efficient industrialized drawing fluids because of their advantages of higher osmotic pressure, easy recycling, and environmentally friendly processes. The types of CO<sub>2</sub>-responsive draw solutions reported thus far mainly include CO<sub>2</sub>-responsive polymer-based draw solutions, CO<sub>2</sub>-responsive hydrogel-based draw solutions, and CO<sub>2</sub>-responsive particle-based draw solutions.

**2.3.1. CO<sub>2</sub>-responsive polymer-based draw solution.** Currently, the most extensively investigated CO<sub>2</sub>-responsive draw solutions are polymer-based. The synthesis strategy relies on living polymerization techniques, that is, free radical polymerization, condensation polymerization, and stepwise polymerization, to polymerize CO<sub>2</sub>-responsive monomers into polymers with CO<sub>2</sub>-responsiveness. This moiety can be a surfactant, monomer, initiator, or a solvent. Compared to CO<sub>2</sub>-

responsive monomers, the CO<sub>2</sub>-responsive polymer form of the draw solution is more chemically and physically stable and can withstand repeated CO<sub>2</sub> stimulation without degradation or structural changes, resulting in stable responsiveness in response to CO<sub>2</sub>, providing stable osmolality, and facilitating recovery.<sup>22–24,26</sup> In addition, the CO<sub>2</sub>-responsive polymer-based draw solution can be adjusted and designed according to needs, for example, by introducing different functional groups or structural units so that the polymer has specific properties in the CO<sub>2</sub> response, such as heat-responsive motifs.<sup>25,33</sup> Thus, it meets practicality requirements in different working scenarios.

**2.3.2. CO<sub>2</sub>-responsive hydrogel-based draw solution.** CO<sub>2</sub>-responsive hydrogels as draw solutions not only exhibit the beneficial properties of conventional hydrogels, such as low toxicity, low reverse salt flux, and high water-absorption capacity,<sup>25,27</sup> but also overcome the limitation of the concentration polarization inherent in conventional draw solutions. Furthermore, these hydrogels effectively balance the seemingly conflicting requirements of high infiltration flux and efficient water recovery during regeneration, making them promising draw solutions for various applications. Currently, the majority of reported CO<sub>2</sub>-responsive hydrogels are synthesized *via* strategies involving Schiff base reactions and chain addition polymerization, such as free radical polymerization.<sup>74–77</sup> This allows the density of CO<sub>2</sub>-responsive sites to be tuned by adjusting the number of CO<sub>2</sub>-responsive motifs within monomers and crosslinkers, thereby influencing the sensitivity of the hydrogel to CO<sub>2</sub>. Furthermore, the type of CO<sub>2</sub>-responsive motif can be strategically selected to optimize the responsiveness of the hydrogel under specific application conditions such as varying temperatures. One point that needs to be emphasized is that, compared with other motifs, amidine CO<sub>2</sub>-responsive hydrogel-based draw solutions suffer from low protonation responsiveness owing to their easy hydrolysis in water.<sup>61,62</sup>

**2.3.3. CO<sub>2</sub>-responsive particle-based draw solution.** CO<sub>2</sub>-responsive particles are generally drawn from organic or inorganic nanoparticles as a support, and CO<sub>2</sub>-responsive monomers are grafted onto the surface of the particles by electrostatic self-assembly or surface chemistry.<sup>78</sup> The grafted layer on the surface of the CO<sub>2</sub>-responsive particles confers a strong CO<sub>2</sub>-responsive function to the modified nanoparticles which leads to a strong osmotic pressure during CO<sub>2</sub>-stimulated protonation and dispersibility in aqueous solvents. During deprotonation by inert gas or heating, the gravity of the internal particle support accelerates the precipitation of the active substance and facilitates its rapid recovery of the active substance. Moreover, when integrated with functional nanoparticles, including magnetic particles and pH-sensitive chromophores, draw solutions can be endowed with enhanced capabilities, such as rapid recovery and real-time pH monitoring. It is important to note that CO<sub>2</sub>-responsive particle-based draw solutions often exhibit lower CO<sub>2</sub>-responsiveness compared to polymer-based and hydrogel-based draw solutions owing to limitations in grafting density.

### 3. Characterization of CO<sub>2</sub>-responsive membrane separation system

CO<sub>2</sub>-responsive materials in membrane separation systems undergo reversible morphological and surface property changes, such as wettability, roughness, and osmotic pressure of the draw solution, when alternately stimulated with CO<sub>2</sub> and inert gases. The accurate characterization of these structural transformations is crucial for elucidating the CO<sub>2</sub>-responsive mechanism and understanding the separation and operation processes of CO<sub>2</sub>-responsive membrane separation systems.

#### 3.1. Characterization of CO<sub>2</sub>-responsive separation membrane

**3.1.1. Wettability.** Reversible protonation/deprotonation cycles in CO<sub>2</sub>-responsive separation membranes enable *in situ* oil–water wettability switching (Fig. 4A). This phenomenon has been characterized using various techniques including contact angle measurements, dynamic adhesion force measurements, and low-field nuclear magnetic resonance (LF-NMR). Contact angle measurement is one of the most commonly used methods for analyzing the wettability change of CO<sub>2</sub>-responsive separation membranes.<sup>79</sup> However, contact angle measurements exclusively provide static and instantaneous wettability information at the fluid–material interface, failing to capture dynamic and long-term interfacial interactions. In contrast, the dynamic adhesion force measurement principle effectively reflects both dynamic and time-dependent wettability changes by quantifying variations in adhesion forces during droplet–surface contact.<sup>80,81</sup> The CO<sub>2</sub>-responsive separation membrane in the dynamic adhesion measurements showed clear gas-

tunable adhesion behavior; that is, it maintained the sphericity of the underwater oil droplet (CO<sub>2</sub> stimulation) and the water droplet under oil (N<sub>2</sub> stimulation) throughout the forward and backward processes (Fig. 4B). In stark contrast, blank membranes without CO<sub>2</sub>-responsive substances exhibited significant shape deformation and force drop during adhesion force measurements, demonstrating a lack of tunable adhesion behavior and the rapid spreading of oil droplets on the membrane surface.

Spectroscopy, a powerful analytical technique that condenses information regarding the structure, properties, and function of a substance, has emerged as a valuable tool for effectively resolving the wettability of membrane materials.<sup>82,83</sup> For example, LF-NMR spectroscopy offers a spectroscopic approach to reveal the oil–water wettability switching mechanism in CO<sub>2</sub>-responsive separation membranes. In LF-NMR (Fig. 4C), a 90° radio frequency pulse aligns molecules in a magnetic field, inducing a transition to a higher-energy state. Upon pulse withdrawal, the aligned molecules relax to their initial state, and the longitudinal relaxation time ( $T_1$ ) and transverse relaxation time ( $T_2$ ) characterize the process. The  $T_1/T_2$  ratio differentiates organic substances ( $>10$ ) from water ( $\approx 1$ ), while  $T_2$  values assess molecular mobility and binding strength. As shown in Fig. 4D, the 2D LF-NMR spectra of the dual-coated fiber (DCF) corresponding membranes provide a detailed mapping of the distribution and extent of both adsorbed and free water and oil phases. This provides the most intuitive information on the reversible oil–water wettability switching of DCF membranes under alternating NIR irradiation and CO<sub>2</sub> stimulation.

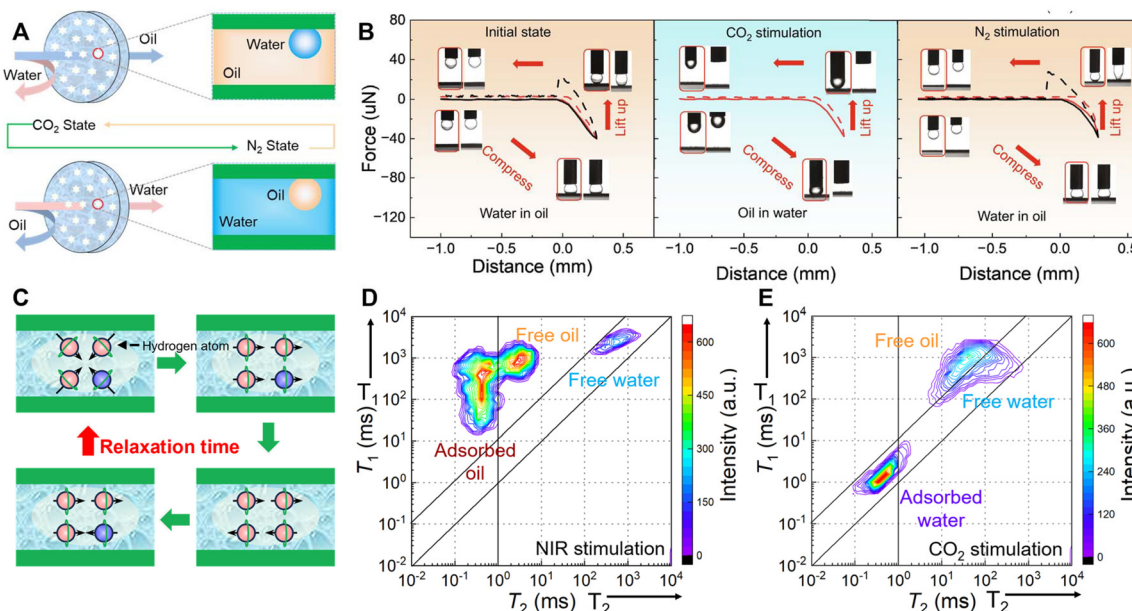


**Fig. 4** Wettability test. (A) Schematic of CO<sub>2</sub> responsive oil–water wettability switching under alternating CO<sub>2</sub> and N<sub>2</sub> atmospheres. (B) Force–distance adhesion curves for water and oil droplets in oil and water environments, comparing the blank membrane (black line) to the CO<sub>2</sub>-RSM membrane (red line) under CO<sub>2</sub>/N<sub>2</sub> stimulation. Reprinted from ref. 55 copyright (2024) with permission from the American Association for the Advancement of Science. (C) Schematic of the LF-NMR test. 2D LF-NMR spectra of the DCF membrane in contact with (D) W/O emulsion under NIR stimulation and (E) O/W emulsion under CO<sub>2</sub> stimulation. Reprinted from ref. 56 copyright (2024) with permission from the Wiley VCH.

**3.1.2. Roughness.** The reversible deprotonation of  $\text{CO}_2$ -responsive separation membranes induces a conformational change in the responsive chain segments from a curled ( $\text{N}_2$ -stimulated) to a straightened ( $\text{CO}_2$ -stimulated) state. This conformational change significantly alters the surface roughness of the membranes, thereby impacting the separation selectivity and resistance to contamination. Currently, atomic force microscopy (AFM) is the most common method used to characterize this change.<sup>84–86</sup> AFM scans the surface of a sample with a sensitive probe and measures the interaction forces (e.g., van der Waals forces and charge forces) between the probe and the surface, thereby obtaining information about the surface topography. Fig. 5a–c illustrate the AFM images of PMMA-*co*-PDEAEMA  $\text{CO}_2$  responsive fibers before and after  $\text{CO}_2$  stimulation, where the surface topography shifted from smooth to rough. Furthermore, techniques such as white-light interferometry and profilometry provide detailed characterization of the membrane surface morphology, including chain conformation and surface defects.<sup>87</sup> These methods enable the generation of 3D images and offer valuable insights into the surface topography.

**3.1.3. Surface potential.**  $\text{CO}_2$ -responsive separation membranes exhibit reversible changes in the surface potential owing to the protonation and deprotonation of functional groups within the membrane matrix.<sup>88,89</sup> Zeta potential ( $\xi$ ) measurements were used to determine the surface charge of the membrane. Generally, when  $\xi$  is high (negative or positive), the repulsive forces between the similarly charged membrane particles are higher than the attractive forces, leading to a more stable membrane structure. Guidelines suggest that

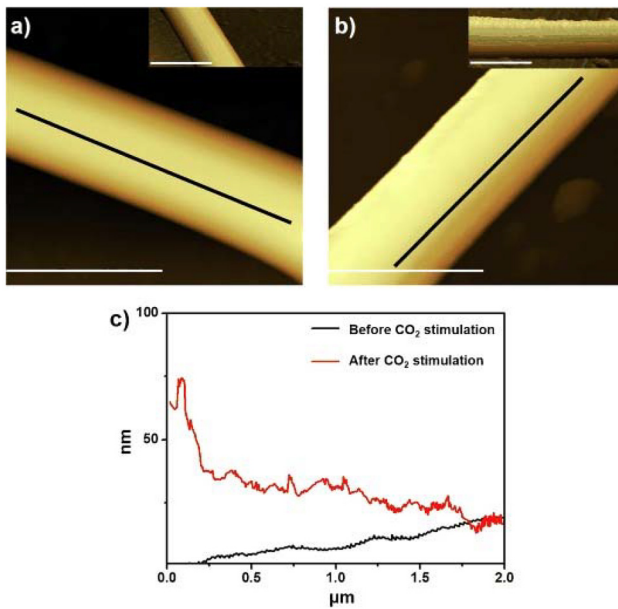


Fig. 5 Roughness test. (a) Before and (b) after  $\text{CO}_2$  stimulations. Insets in (a) and (b) are the corresponding 3D AFM images. (c) Surface roughness curve of a single nanofiber in the absence and presence of  $\text{CO}_2$ . Reprinted from ref. 37 copyright (2019) with permission from American Chemical Society.

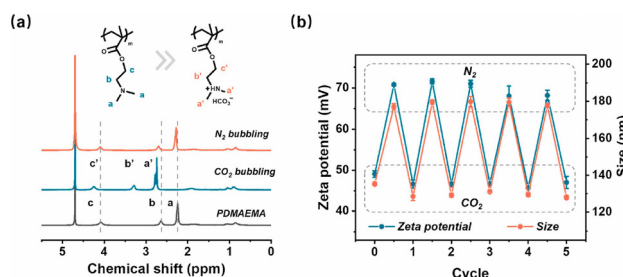


Fig. 6 Surface potential test. (a) Chemical shifts in PDMAEMA after the alternative stimulation of  $\text{CO}_2/\text{N}_2$ . (b) Zeta potentials of PDMAEMA-*b*-PS micelles after the cyclic stimulation of  $\text{CO}_2/\text{N}_2$ . Reprinted from ref. 31 copyright (2019) with permission from American Chemical Society.

membrane systems with an absolute value  $|\xi| > 30$  mV are highly stable, whereas those with  $|\xi|$  within the range of 20–30 mV are moderately stable. In contrast, membranes with  $|\xi|$  values within the range of 10–20 mV and 0–10 mV are mostly unstable and completely unstable, respectively. Fig. 6 demonstrates that alternating  $\text{CO}_2/\text{N}_2$  stimulation induced reversible changes in the charge properties of the PDMAEMA-*b*-PS  $\text{CO}_2$ -responsive membranes, with the zeta potential reversibly switching between values below 75 mV and above 40 mV. Remarkably, this  $\text{CO}_2$ -driven membrane potential reversal pattern was stable over five consecutive cycles.

### 3.2. Characterization of $\text{CO}_2$ -responsive draw solutions

**3.2.1. Osmotic pressure.** Osmotic pressure is a critical parameter in  $\text{CO}_2$ -responsive draw solution applications and influences selectivity in forward osmosis systems and water flux.<sup>24</sup> Freezing point depression ( $\Delta T_f$ ), a colligative property, is a reliable method for determining solute concentration and osmotic pressure indirectly (Fig. 7A and B). The temperature at which a solution begins to freeze relative to a pure solvent is given by the equations

$$\Delta T_f = K_f \cdot m$$

and

$$\pi = iMRT$$

where  $K_f$  is the cryoscopic constant and  $i$  is the van't Hoff factor defined as the ratio of the actual particle concentration produced by the dissolved substance to the concentration calculated based on its mass. For instance, the ideal electrolyte  $\text{NaCl}$  ( $i = 2$ ) dissociates into two ions ( $\text{Na}^+$  and  $\text{Cl}^-$ ) per molecule, while the nonelectrolyte glucose ( $i = 1$ ) does not dissociate.  $M$  is molarity,  $R$  is the gas constant, and  $T$  is temperature. Precise osmotic pressure estimates can be obtained for solutions with low to moderate solute concentrations. Utilizing this approach, draw solutions incorporating each of the three  $\text{CO}_2$ -responsive branched polymers at a concentration of 43 wt/vol% exhibited ultrahigh osmotic pressures exceeding 67 bar under  $\text{CO}_2$  stimulation (Fig. 7B). Notably, these osmotic pressures were 2.5 times greater than those of ordinary baseline seawater (27 bar).

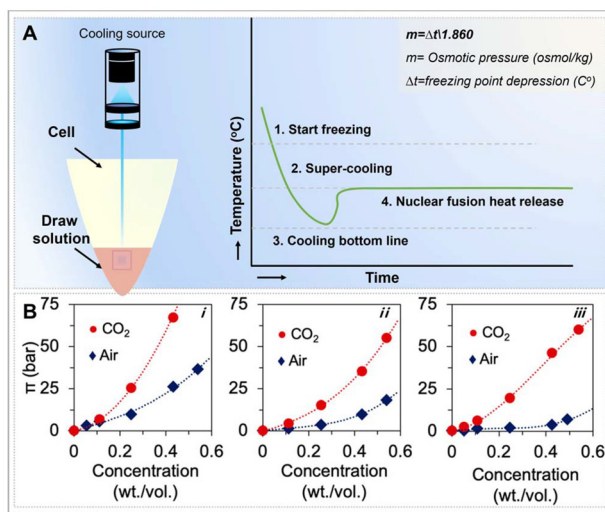


Fig. 7 Osmotic pressure test. (A) Schematic of the freezing point depression method used to test osmolality. (B) Osmotic pressure of aqueous solutions of amine-based polymers under air and CO<sub>2</sub> as a function of polymer mass fraction: (i) linear PMEI, (ii) branched PMEI, and (iii) PDMAAm. Reprinted from ref. 26 copyright (2024) with permission from the American Chemical Society.

**3.2.2. Solubility.** The alternating CO<sub>2</sub>/N<sub>2</sub> action of CO<sub>2</sub>-responsive raw solutions produces, in addition to a change in osmotic pressure, a simultaneous reversal of the solubility of CO<sub>2</sub>-responsive substances, that is, the dissolution and precipitation of CO<sub>2</sub>-responsive substances.<sup>90–92</sup> UV spectrophotometry monitoring of transmittance changes can be used to accurately characterize the reversible responsiveness (Fig. 8). In the time-transmittance mode, a wavelength unaffected by the CO<sub>2</sub>-responsive material is selected. When protonated in water, the CO<sub>2</sub>-responsive active material dissolved well, resulting in a clear solution with high transmittance. During recovery, as the active material shifted from hydrophilic to hydro-

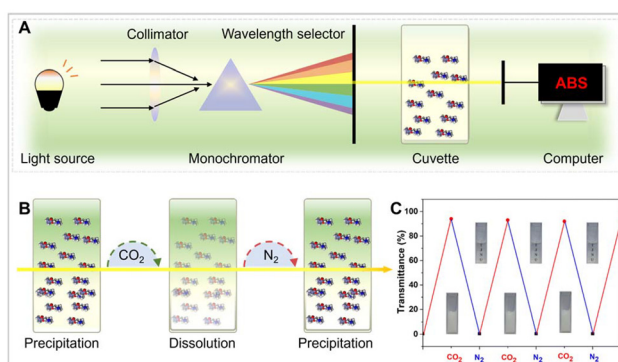


Fig. 8 Solubility test. (A) Schematic of the UV spectrophotometry method used to test solubility. (B) Schematic of liquid transmittance in the presence of different gases for sol-intelligent switching. (C) Change in the transmittance of the P(Ph-N-EO<sub>2</sub>MA) aqueous solution at 28 °C upon N<sub>2</sub>/CO<sub>2</sub> bubbling. Reprinted from ref. 91 copyright (2024) with permission from the Royal Society of Chemistry.

phobic, the solution became turbid, leading to decreased transmittance. This method provides a rapid assessment of the responsiveness and recyclability of CO<sub>2</sub>-responsive draw solutions.

## 4. Applications of CO<sub>2</sub>-responsive membrane separation system

Upon realizing the potential of designing CO<sub>2</sub>-responsive materials, a plethora of innovative applications and novel concepts have emerged. The following section highlights the applications of CO<sub>2</sub>-responsive membrane separation systems and outlines the directions for future development.

### 4.1. Oil–water separation

Oily wastewater is toxic and hazardous, causing serious environmental pollution and health risks.<sup>93,94</sup> Membrane-based oil–water separation has emerged as the preferred solution for treating oily wastewater. Nevertheless, most traditional membranes exhibit a single and unalterable wettability, which severely limits their application to actual oil/water mixtures with the coexistence of different types of immiscible and emulsified mixtures. CO<sub>2</sub>-responsive membranes with tunable wettability offer a promising approach for addressing these challenges. Fig. 9 illustrates a CO<sub>2</sub>-responsive nanofiber membrane fabricated *via* the electrospinning of a PMMA-*co*-DEAEMA polymer blend. The incorporation of the PMMA units ensured the insolubility of the nanofibers in water. The intertwining and interlocking of the nanofiber network resulted in a loose,

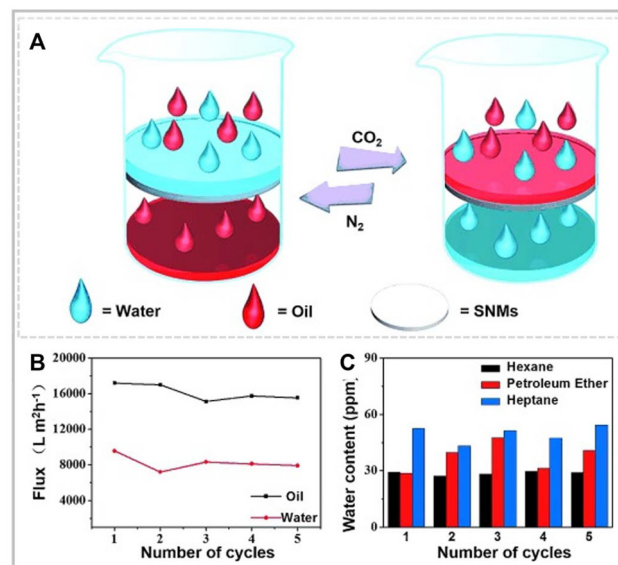


Fig. 9 Oil–water mixture separation. (A) Representation of CO<sub>2</sub> responsive oil/water on–off switch. (B) Variations in the fluxes of oil and water in the absence and presence of CO<sub>2</sub>. (C) Water content of the oil in the filtrate after permeation of the oil/water mixtures through the CO<sub>2</sub>-responsive nanofiber membrane. Reprinted from ref. 37 copyright (2015) with permission from Wiley VCH.

interconnected membrane structure, a reduced mass transfer resistance, and an enhanced  $\text{CO}_2$  responsiveness. Upon the introduction of  $\text{CO}_2$ , the tertiary amine groups in PDEAEMA underwent protonation, inducing a hydrophilic state in the nanofibrous membrane and facilitating rapid water permeation (>9554 LMH). Conversely, under  $\text{N}_2$  stimulation, deprotonation of PDEAEMA and the roughness of the nano-fiber network contributed to a hydrophobic state, enabling rapid oil transport (>17 000 LMH).

The separation of complex oil-water emulsions involves not only wettability but also size-screening effects.<sup>95,96</sup> This necessitates advanced fabrication techniques with precise molecular-level design to achieve selectivity for small oil-water emulsions. To address this challenge, RSM was fabricated using core-shell fibers with a  $\text{CO}_2$ -responsive PMMA-*co*-PDEAEMA shell. Advanced industrial weaving techniques enabled the creation of RSMs with adjustable pore sizes ranging from 0.2 to 1.5  $\mu\text{m}$  by controlling packing density and the number of sizing cycles. These membranes can subsequently be encapsulated into modules for the separation of oil-water emulsions (Fig. 10). Upon  $\text{CO}_2$  treatment, the RSM transitions from a hydrophobic to a hydrophilic state. This enabled rapid water permeation (1000 LMH) while retaining the oil phase in the oil-in-water emulsions. Conversely,  $\text{N}_2$  treatment restored the hydrophobic state, facilitating rapid oil

permeation (1000 LMH) while retaining the water phase in the water-in-oil emulsions. This versatility extends to a wide range of oil-water systems, including those involving light oils (*e.g.*,  $n$ -hexane, isooctane) and high-viscosity oils (*e.g.*, silicone oil, soybean oil, olive oil, and crude oil). By simply alternating the  $\text{CO}_2/\text{N}_2$  treatments, RSM achieved a separation efficiency of more than 99.6%.

#### 4.2. Molecular separation

In industrial production, particularly in life science applications such as protein and polysaccharide purification, there is a strong demand for mild, low-toxicity separation methods.<sup>48,97,98</sup> Conventional stimulus-responsive (*e.g.*, pH, heat, light, and electricity) separation membranes have major limitations in applying these triggers, including economic and environmental costs and product contamination.  $\text{CO}_2$ -responsive separation membranes, characterized by their nontoxicity, inexpensiveness and mild response, offer a promising solution. The membrane pore size is dynamically adjusted in response to  $\text{CO}_2$ , enabling the effective separation of molecules based on their size differences. Furthermore, during this process, no by-products are generated that could compromise the membrane structure, thereby ensuring sustained high-performance separation. Wang *et al.* successfully fabricated a  $\text{CO}_2$ -responsive PDEAEMA-*b*-PS membrane on a PVDF substrate by spin-coating. Upon  $\text{CO}_2$  stimulation, protonation of the tertiary amine groups within PDEAEMA increased the hydrophilicity and extended the polymer chains, reducing the mean pore size from 162 to 60 nm.<sup>48</sup> This effect was reversible upon  $\text{N}_2$  stimulation. This reversible pore size response enables precise control of protein passage, achieving tight ultrafiltration with a minimum pore size of 4.2 nm and a high separation efficiency of 97% for biomolecule pairs, such as bacitracin and lysozyme. The membrane also exhibited excellent response stability for biomolecule pairs over five  $\text{CO}_2/\text{N}_2$  cycles.

Further studies have found that  $\text{CO}_2$ -responsive separation membranes offer a potential solution for membrane contamination. Upon protonation, the conformation of the responsive chain segments shifted from a curled to a straightened state, isolating the membrane surface from direct solute contact and reducing fouling during the separation process. For instance, as shown in Fig. 11, Zhang *et al.* fabricated PVDF/PDEAEMA composite membranes using a blade-coating method. The incorporation of  $\text{CO}_2$ -responsive PDEAEMA into the PVDF matrix increased the hydrophobicity.<sup>44</sup> However, upon  $\text{CO}_2$  stimulation, protonation of the PDEAEMA chains induces a hydrophilic transition, significantly enhancing the water flux. More importantly, the conformational change of  $\text{CO}_2$ -responsive segments from a collapsed to an extended state during protonation can effectively prevent protein adsorption and deposition on the membrane surface, resulting in a high flux recovery rate of 95% for the PVDF/PDEAEMA membrane compared to 56% for pure PVDF membranes after pure water backwashing.

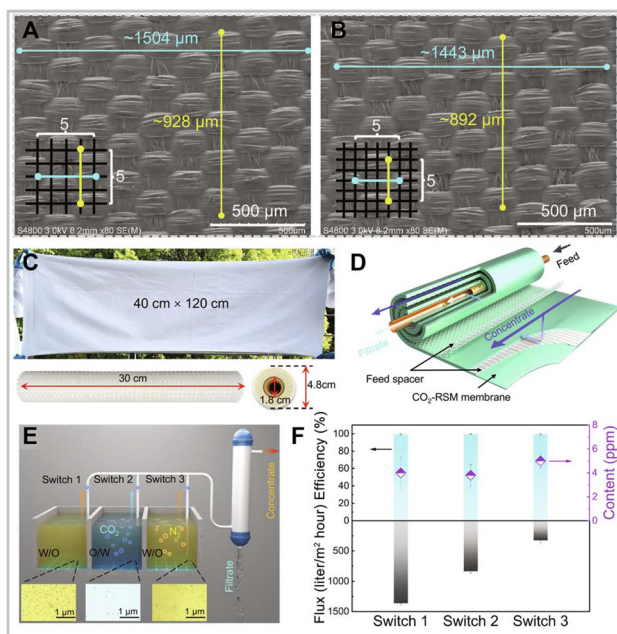


**Fig. 10** Oil-water emulsion separation. Surface SEM images of  $\text{CO}_2$ -RSM with low (A) and high (B) weaving densities. (C) Photograph of a spiral-wound membrane module showing a large-sized  $\text{CO}_2$ -RSM membrane. (D) Schematic representation of the spiral-wound module. (E) Schematic showing the continuous and switchable separation performance of the  $\text{CO}_2$ -RSM module in different nanoemulsion systems. (F) Separation efficiency of the  $\text{CO}_2$  RSM membrane module in different switch states. Reprinted from ref. 55 copyright (2024) with permission from the American Association for the Advancement of Science.

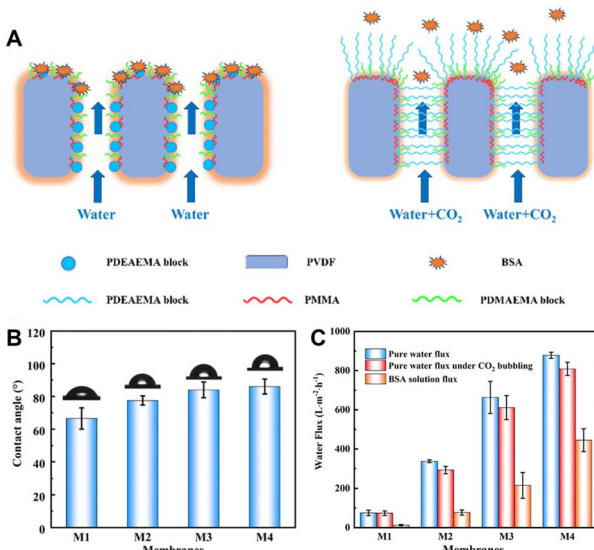


Fig. 11 Molecular separations. (A) Schematic of the CO<sub>2</sub>-responsive separation mechanism of PVDF blend membranes. (B) Water contact angles and (C) water flux performance of the membranes prepared with different amounts of PDEAEMA. Reprinted from ref. 46 copyright (2024) with permission from Wiley VCH.

#### 4.3. Ion separation

Ion separation is crucial for various applications, including seawater desalination, lithium extraction from saline lakes, and boiler feedwater treatment.<sup>99,100</sup> However, most conventional nanofiltration membranes are mono-charged (positively or negatively), showing high rejection only for the corresponding co-ions but low rejection for the counter-ions, which limits their wider applications. CO<sub>2</sub>-responsive membranes undergo protonation upon CO<sub>2</sub> exposure, allowing reversible changes in the pore size and charge state of the membrane. This dual mechanism, which combines size-based sieving and the Donnan effect, enables the development of highly efficient and selective nanofiltration membranes. Zhao *et al.* fabricated a Py-PDEAEMA/GO membrane *via* vacuum filtration by integrating GO with a CO<sub>2</sub>-responsive polymer, poly(2-(diethylamino)ethyl methacrylate) (Py-PDEAEMA).<sup>38</sup> Under CO<sub>2</sub> stimulation, protonation of CO<sub>2</sub>-responsive polymer chains within the Py-PDEAEMA/GO membrane enhances pore channel wettability and significantly increases permeability. This effect is amplified by increasing the molecular weight of Py-PDEAEMA, as the polymer contributes to the increased interlayer spacing in GO, reducing the diffusion resistance. Additionally, CO<sub>2</sub>-induced protonation of Py-PDEAEMA imparts a high positive potential to the membrane surface, enhancing the retention capacity of the positively charged salt ions in the Py-PDEAEMA/GO membranes. This effect was demonstrated by an increase in magnesium ion retention from 5% to 45% (Fig. 12).

Zhao *et al.* subsequently developed a CO<sub>2</sub>-responsive GO/Py-PDMAEMA membrane with invertible surface potential. The membrane was fabricated *via* self-assembly of GO and hydro-

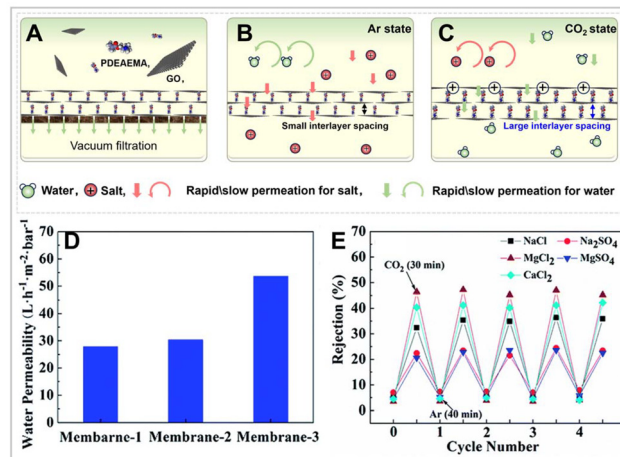


Fig. 12 Ion separation. (A–C) Schematic representation of the preparation and separation process of the Py-PDEAEMA/GO membrane. (D) Water permeability of the Py-PDEAEMA/GO membranes prepared with different molecular weights of Py-PDEAEMA. (E) Responsive rejection stability of salts in water by Py-PDEAEMA/GO membranes over five CO<sub>2</sub>/N<sub>2</sub> cycles. Reprinted from ref. 38 copyright (2018) with permission from the Royal Society of Chemistry.

philic Py-PDMAEMA, followed by vacuum filtration (Fig. 13).<sup>88</sup> The hydrophilic nature of Py-PDMAEMA ensures that its responsive groups remain in a stretched state under both protonation and deprotonation, eliminating the influence of pore size variation on the nanofiltration performance of the membrane. This emphasizes the dominant role of the Donnan effect in nanofiltration. In accordance with the Donnan exclusion theory, the Donnan potential established at the solution–membrane interface electrostatically repels co-ions sharing the

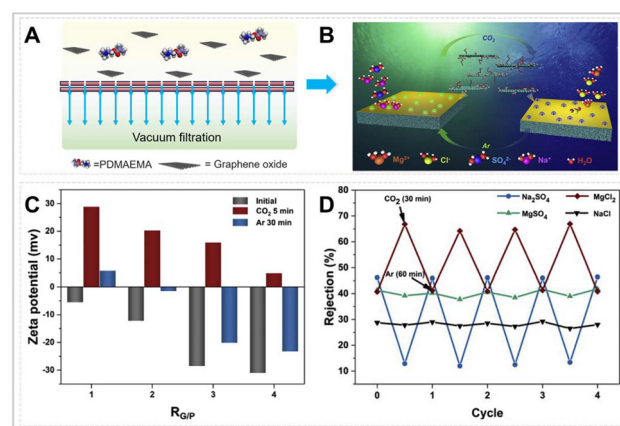


Fig. 13 Ionic separation based on the Donnan effect. (A and B) Schematic of the preparation and separation of the GO/Py-PDMAEMA/PVDF membrane. (C) Variation in the zeta potential of GO/Py-PDMAEMA dispersion with different RG/P ratios after CO<sub>2</sub> bubbling (5 min) and subsequent Ar bubbling (30 min). (D) Responsive rejection stability of salts in water for the GO/Py-PDMAEMA/PVDF membranes over five CO<sub>2</sub>/N<sub>2</sub> cycles. Reprinted from ref. 88 copyright (2019) with the permission of Elsevier.

charge of the membrane. Consequently, negatively charged membranes exhibit a higher rejection rate for salts with divalent co-ions (e.g.,  $\text{SO}_4^{2-}$  in  $\text{Na}_2\text{SO}_4$ ) than for those with monovalent co-ions (e.g.,  $\text{Cl}^-$  in  $\text{NaCl}$ ). Conversely, salts containing divalent counterions (e.g.,  $\text{Ca}^{2+}$  in  $\text{CaCl}_2$ ) are rejected less effectively than those containing monovalent counterions (e.g.,  $\text{Na}^+$  in  $\text{NaCl}$ ). Specifically, the GO/Py-PDMAEMA membrane underwent reversible protonation and deprotonation upon alternating exposure to  $\text{CO}_2$  and  $\text{N}_2$ , inducing a reversible shift in the membrane surface potential between  $-30$  and  $+30$  mV. This enables the on-demand separation of salt ions by the GO/Py-PDMAEMA membrane, which is consistent with the Donnan exclusion theory, as follows.

$$R = 1 - \frac{C_B^m}{C_B} = \left( \frac{|Z_B|C_B}{|Z_B|C_B^m + C_X^m} \right)^{|Z_B|/|Z_A|}$$

Here,  $Z_A$  and  $Z_B$  are the valences of the counter-ions and co-ions, respectively, relative to the membrane charge.  $C_B$  and  $C_B^m$  denote the co-ion concentrations in the solution and membrane phase, respectively, and  $C_X^m$  denotes the concentration of membrane surface charges.

#### 4.4. Forward osmosis system

In contrast to nanofiltration, ultrafiltration, and other pressure-driven membrane processes, FO operates based on an osmotic pressure gradient between the feed and draw solutions, eliminating the need for external pressurization.<sup>101,102</sup> This inherent characteristic renders FO an inherently green and energy-efficient separation technology that has found applications in diverse fields, including seawater desalination, pharmaceutical desalting, and food concentration. The performance of FO systems is significantly influenced by the type and concentration of the draw solution, which directly affect the water flux, contaminant rejection, and energy efficiency. Compared with conventional inorganic salt- and other stimulus-responsive draw solutions,  $\text{CO}_2$ -responsive draw solutions exhibit superior recyclability and reusability owing to their non-toxic, harmless, and mild processing conditions.  $\text{CO}_2$ -responsive draw solutions also exhibit high osmotic pressures in the protonated states and are easy to recover in the deprotonated state, which has led to widespread interest and research. In 2013, Hu *et al.* first reported the application of  $\text{CO}_2$ -responsive draw solutes (PDMAEMA) in FO systems.<sup>23</sup> Under  $\text{CO}_2$  stimulation, this draw solute underwent protonation, achieving an osmolality of  $1.208 \text{ Osmol kg}^{-1}$ , nearly four times that of seawater, and demonstrated a high salt rejection rate of 96% (NaCl) in desalination experiments.

The conventional recovery process for  $\text{CO}_2$ -responsive draw solutions, involving deprotonation and precipitation, disrupts continuous FO operation and reduces the separation efficiency. Therefore, rapid draw-solution recovery is critical for achieving efficient and uninterrupted FO processes. Dual-responsive draw solutes, such as those exhibiting  $\text{CO}_2$  and thermo or magnetic responsiveness, have been developed to

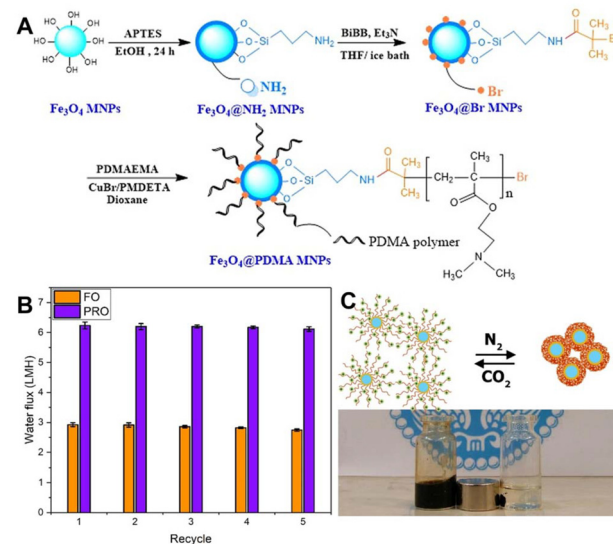


Fig. 14 Draw solution. (A) Schematic of grafting PDMA chains onto the surface of  $\text{Fe}_3\text{O}_4\text{-Br}$  by ATRP. (B) Recycling test of  $\text{Fe}_3\text{O}_4\text{@PDMA-12}$  water flux in FO and PRO modes. (C) Quick  $\text{CO}_2$ -magnetic response performance of  $\text{Fe}_3\text{O}_4\text{@PDMA-12}$ . Reprinted from ref. 78 copyright (2022) with permission from Elsevier.

address this challenge and enable rapid draw solution collection. Shakeri *et al.* demonstrated this approach by synthesizing a  $\text{CO}_2$  and magnetically responsive dual-purpose draw solute (Fig. 14A).<sup>78</sup> This material features PMMA grafted onto magnetic  $\text{Fe}_3\text{O}_4$  nanoparticles. Under  $\text{CO}_2$  stimulation, PMMA generates a high osmotic pressure, while the magnetic properties of  $\text{Fe}_3\text{O}_4$  facilitate a significantly faster draw solution recovery process, reducing the time cycle threefold. Notably, the recovered draw solution exhibited consistent water flux stability over five reuse cycles (Fig. 14B and C).

## 5. Challenge and outlook

$\text{CO}_2$ -responsive materials, owing to their ease of processing and green mode of action, have seen significant development and application in membrane systems in recent years, and now is a good time to assess their progress, particularly in terms of commercialization and large-scale implementation. To the best of our knowledge, no industrialised  $\text{CO}_2$ -responsive membrane separation systems have been established, although we are aware that several companies are actively pursuing developments involving  $\text{CO}_2$ -responsive draw solutions and  $\text{CO}_2$ -responsive separation membranes for the separation of emulsified wastewater from oilfields. Recently, there has been a surge in the development of  $\text{CO}_2$ -responsive membrane systems driven by the proliferation of  $\text{CO}_2$ -responsive materials and a deepening understanding of their underlying mechanisms. However, significant challenges persist in the advancement of these systems.

(i) The scaled-up preparation of CO<sub>2</sub>-responsive materials, including membrane materials and draw solutions, is key to achieving the separation potential of CO<sub>2</sub>-responsive separation systems in industrial applications. For CO<sub>2</sub>-responsive separation membranes, although small-area membrane samples can be prepared in a variety of ways in the laboratory, a preparation scheme that allows continuous large-scale preparation of CO<sub>2</sub>-responsive membranes has yet to be reported. In contrast, research on nanofiltration membranes commenced earlier, and several schemes for the preparation of large-area nanofiltration membranes have been reported.<sup>103–106</sup> Notably, some of these schemes are also applicable for the preparation of CO<sub>2</sub>-responsive membranes, potentially contributing to their large-scale production. Furthermore, considering the operational costs of CO<sub>2</sub> responsive separation membranes after large-scale industrialisation, subsequent research should conduct comparative analyses of the energy efficiency, energy consumption, and costs of CO<sub>2</sub> responsive separation membranes with other stimulus-responsive separation membranes. This highlights the environmental and energy-saving advantages of CO<sub>2</sub> responsive separation membranes. For example, the equipment operation energy consumption of thermo-responsive separation membranes in the industry is 9500 kWh m<sup>-3</sup>, which is lower than that of commercial membranes.<sup>107</sup> Therefore, the economic performance of CO<sub>2</sub> responsive separation membranes is also a key factor in determining whether they can be industrially mass-produced on a large scale. For CO<sub>2</sub>-responsive draw solutions, the synthesis process often requires an inert atmosphere and involves intricate synthetic pathways, thereby posing a significant barrier to large-scale manufacturing. It is interesting to note that air-tolerant polymerization techniques, such as emulsion polymerization, demonstrated in preliminary studies for CO<sub>2</sub>-responsive draw solutions, offer promising avenues for overcoming this limitation.

(ii) Disregarding diffusional limitations, CO<sub>2</sub>-responsive systems generally exhibit longer switching times compared to other stimuli, such as pH, heat, or light, which often results in membrane systems failing to achieve a continuous and efficient separation process.<sup>108</sup> For example, the CO<sub>2</sub> inflation time is 15 minutes, and the N<sub>2</sub> inflation time is 30 minutes. To overcome this, strategies to accelerate CO<sub>2</sub>-responsiveness are crucial. Incorporating hydrophobic groups such as branched chains (*e.g.*, phenyl) into CO<sub>2</sub>-responsive motifs can reduce the pK<sub>a</sub> value, facilitating deprotonation. Additionally, third-party responsiveness can be integrated into CO<sub>2</sub>-responsive membrane systems, such as GO to accelerate deprotonation *via* near-infrared light-induced photothermal conversion.

(iii) A CO<sub>2</sub>-responsive membrane separation system requires the addition or removal of gaseous CO<sub>2</sub> in neutral water, which requires effective mass transfer through the system in question. This process involves initial macroscopic mixing driven by convective flow, followed by molecular diffusion to bring the gas into proximity with the membrane surface, enabling performance switching. However, a liquid medium with high viscosity (such as heavy oil) can significantly hinder

gas dispersion, potentially requiring unreasonably long times to achieve effective mixing.<sup>109,110</sup> Future research should focus on analyzing the reaction kinetics and fluid dynamics by varying the gas delivery conditions to gain a deeper understanding of the protonation and deprotonation processes in CO<sub>2</sub>-responsive membranes, enabling more efficient and controlled operation.

(iv) In most published studies, CO<sub>2</sub> is introduced into membrane systems *via* bubbling, with limited attention given to quantifying key parameters, such as flow rates, partial pressures in the headspace, or the molar ratio between CO<sub>2</sub> and the responsive components. This lack of quantification hinders the accurate assessment of CO<sub>2</sub> utilization efficiency and poses economic challenges. Therefore, it is necessary to establish a clear relationship between the CO<sub>2</sub> input and membrane system parameters (*e.g.*, membrane area, draw solution volume, and concentration), particularly for the development of large-scale industrial applications of CO<sub>2</sub>-responsive membrane systems. For industrial-grade nanofiltration/ultrafiltration systems, which typically use a closed-loop staggered-flow filtration mode, intelligent control can be achieved by integrating a CO<sub>2</sub>/N<sub>2</sub> dual-gas path-switching system into the feed line. Specifically, a parallel dual-channel gas-bubbling device was installed upstream of the membrane module. This allows the CO<sub>2</sub>-responsive membrane to reversibly switch between the protonated and deprotonated states *via* periodic alternating injections of CO<sub>2</sub> and N<sub>2</sub>. For industrial-scale forward osmosis systems, continuous draw-solution circulation is essential for maintaining a high osmotic pressure, and a CO<sub>2</sub>/N<sub>2</sub> dual-gas path switching system can be integrated into the draw-solution recirculation line. This involves adding a parallel dual-channel gas-bubbling device to the circulating pipeline. By periodically switching between alternating CO<sub>2</sub> and N<sub>2</sub> injections, the CO<sub>2</sub>-responsive draw solution can be reversibly switched between protonated and deprotonated states, thereby dynamically regulating the osmotic pressure and enhancing the separation efficiency. Additionally, strategies for achieving cyclic utilization of CO<sub>2</sub> in the whole response process are effective approaches to reducing CO<sub>2</sub> procurement costs and emissions.

(v) CO<sub>2</sub>-responsive motifs, such as guanidine and imidazole, exhibit a stable protonated state owing to their high pK<sub>a</sub> values. This hinders deprotonation through conventional gas bubbling, necessitating alternative methods, such as heating. Consequently, the application of guanidine and imidazole CO<sub>2</sub>-responsive materials in membrane systems is limited. Nevertheless, these characteristics make them highly promising for high-temperature separation processes such as vapor permeation and wastewater filtration for the textile industry.<sup>111–114</sup>

(vi) Although CO<sub>2</sub>-responsive membrane separation systems exhibit broad applicability, their implementation in complex separation scenarios, such as those encountered in fermentation broths and petrochemical emulsions, necessitates a meticulous assessment of the influence of impurities and solvent properties, particularly the pH level.<sup>115,116</sup> A tailored approach

is crucial to mitigate the detrimental effects of impurities. This may involve incorporating pre-crude separation processes or employing a pH buffer to minimize interference with the CO<sub>2</sub>-responsive membrane system. Additionally, CO<sub>2</sub>-responsive membrane separation systems represent one branch of CO<sub>2</sub>-responsive system applications. Other major application areas include CO<sub>2</sub>-responsive adsorbent materials and CO<sub>2</sub>-responsive sensing materials. Given that CO<sub>2</sub>-responsive systems across these diverse fields share a common response mechanism, there is a significant mutual reference value in their preparation methods, response forms, and characterization techniques. This cross-application potential can further enrich the available options for CO<sub>2</sub>-responsive membrane systems in the future.

## 6. Conclusions

CO<sub>2</sub>-responsive membrane separation systems have garnered significant attention owing to their ability to achieve controlled and efficient separation processes. Significant progress has been made in the design, fabrication, and applications of these systems, demonstrating their potential for environmental and industrial applications. However, several challenges remain for the large-scale implementation of CO<sub>2</sub>-responsive membrane separation systems, including optimization of the CO<sub>2</sub> utilization efficiency, scalability of membrane fabrication, and integration of these systems into industrially relevant conditions. Future research should focus not only on improving the responsiveness and stability of CO<sub>2</sub>-responsive materials, but also on addressing practical challenges such as energy efficiency, CO<sub>2</sub> recovery, and system scalability. By tackling these issues, CO<sub>2</sub>-responsive membrane systems hold great promise for advancing sustainable separation technologies and supporting global carbon management.

## Author contributions

L. L., H. L. and L. D.: Original drafting of the whole document. L. L. and H. L.: Conceptualization and drafting. L. L. and H. L.: Developing the figures and tables, collecting references, and formatting the manuscript as per the guidelines of the journal. L. L., Y. B., C. Z., M. Y. and W. W.: Editing and proofreading the manuscript. L. D.: Supervision, reviewing, and updating the whole document.

## Conflicts of interest

The authors declare that they have no known conflicting financial interests or personal ties that might have influenced the work presented in this study.

## Data availability

No primary data were used in this article. This means that no primary research results, software, or codes are included, and no new data were generated or analyzed as part of this review.

## Acknowledgements

This work was financially supported by the National Key Research and Development Program of China (2024YFB3815500), the National Science Foundation of Jiangsu Province (BK20230106), Fundamental Research Funds for the Central Universities (JUSR622035), the Natural Science Foundation of Xinjiang Uygur Autonomous Region (2022D01D030).

## References

- 1 Z. Liu, W. Wang, R. Xie, X. J. Ju and L. Y. Chu, *Chem. Soc. Rev.*, 2016, **45**, 460–475.
- 2 S. Overmans, G. Ignacz, A. K. Beke, J. Xu, P. E. Saikaly, G. Szekely and K. J. Lauersen, *Green Chem.*, 2022, **24**, 5479–5489.
- 3 A. Colom, E. Derivery, S. Soleimanpour, C. Tomba, M. D. Molin, N. Sakai, M. González-Gaitán, S. Matile and A. Roux, *Nat. Chem.*, 2018, **10**, 1118–1125.
- 4 T. Huang, Z. Su, K. Hou, J. Zeng, H. Zhou, L. Zhang and S. P. Nunes, *Chem. Soc. Rev.*, 2023, **52**, 4173–4207.
- 5 D. Yu, X. Xiao, C. Shokoohi, Y. Wang, L. Sun, Z. Juan, M. J. Kipper, J. Tang, L. Huang, G. S. Han, H. S. Jung and J. Chen, *Adv. Funct. Mater.*, 2023, **33**, 2211983.
- 6 D. L. Keshebo, H. F. Darge, C. C. Hu, H. C. Tsai, C. J. Su, Y. M. Sun, W. S. Hung, C. F. Wang, K. R. Lee and J. Y. Lai, *J. Membr. Sci.*, 2022, **664**, 121080.
- 7 L. Zheng, M. Ulbricht, B. Van der Bruggen, Z. Wang, D. Hou and Y. Wei, *Water Res.*, 2024, **249**, 120939.
- 8 Z. Zhang, X. Xiao, Y. Zhou, L. Huang, Y. Wang, Q. Rong, Z. Han, H. Qu, Z. Zhu, S. Xu, J. Tang and J. Chen, *ACS Nano*, 2021, **15**, 13178–13187.
- 9 X. X. Fan, R. Xie, Q. Zhao, X. Y. Li, X. J. Ju, W. Wang, Z. Liu and L. Y. Chu, *J. Membr. Sci.*, 2018, **555**, 20–29.
- 10 P. Das, N. D. Benizio, S. Desclaux, C. Causserand, J. C. Remigy, J. F. Lahitte, V. Pimienta, C. Coudret and C. Coetsier, *Chem. Eng. J.*, 2024, **500**, 157337.
- 11 Q. Ye, R. Wang, S. Yan, B. Chen and X. Zhu, *J. Mater. Chem. B*, 2022, **10**, 2617–2627.
- 12 H. Zhang, J. Miao, X. Ning and T. Fan, *Desalination*, 2024, **592**, 118163.
- 13 Q. Chen, J. Liu, L. Tang, Z. Zeng and B. Zhu, *J. Environ. Chem. Eng.*, 2024, **12**, 112422.
- 14 B. G. Molina, H. Enshai, A. Gil, P. A. Haro-Gutierrez, L. Resina, M. Sánchez-Jiménez and C. Alemán, *Polymer*, 2024, **311**, 127535.
- 15 J. Xing, H. Zhang, G. Wei, T. Hong, S. Chen, H. Liang and X. Quan, *Chem. Eng. J.*, 2024, **494**, 153218.

16 L. Dong and Y. Zhao, *J. Mater. Chem. A*, 2020, **8**, 16738–16746.

17 A. Darabi, P. G. Jessop and M. F. Cunningham, *Chem. Soc. Rev.*, 2016, **45**, 4391–4436.

18 R. D. Jansen-van Vuuren, S. Naficy, M. Ramezani, M. Cunningham and P. Jessop, *Chem. Soc. Rev.*, 2023, **52**, 3470–3542.

19 M. F. Cunningham and P. G. Jessop, *Macromolecules*, 2019, **52**, 6801–6816.

20 Q. Yan and Y. Zhao, *Chem. Commun.*, 2014, **50**, 11631–11641.

21 Z. Yang, C. He, H. Sui, L. He and X. Li, *J. CO<sub>2</sub> Util.*, 2019, **30**, 79–99.

22 A. Riabtseva, S. N. Ellis, P. Champagne, P. G. Jessop and M. F. Cunningham, *Ind. Eng. Chem. Res.*, 2021, **60**, 9807–9816.

23 Y. Cai, W. Shen, R. Wang, W. B. Krantz, A. G. Fane and X. Hu, *Chem. Commun.*, 2013, **49**, 8377–8379.

24 S. N. Ellis, A. Riabtseva, R. R. Dykeman, S. Hargreaves, T. Robert, P. Champagne, M. F. Cunningham and P. G. Jessop, *Ind. Eng. Chem. Res.*, 2019, **58**, 22579–22586.

25 S. N. Ellis, M. F. Cunningham and P. G. Jessop, *Desalination*, 2021, **510**, 115074.

26 J. Frauholz, M. F. Cunningham and P. G. Jessop, *Ind. Eng. Chem. Res.*, 2024, **63**, 10713–10720.

27 H. Rabiee, B. Jin, S. Yun and S. Dai, *Chem. Eng. J.*, 2018, **347**, 424–431.

28 D. Tao, Z. Qi, Q. Gao, Y. Liu, J. Guo and Y. Yu, *Surf. Interfaces*, 2023, **36**, 102542.

29 L. Lei, Q. Zhang, S. Shi and S. Zhu, *Langmuir*, 2017, **33**, 11936–11944.

30 Q. Zhang, Z. Wang, L. Lei, J. Tang, J. Wang and S. Zhu, *ACS Appl. Mater. Interfaces*, 2017, **9**, 44146–44151.

31 C. Zhang, J. Zhou, X. Ye, Z. Li and Y. Wang, *J. Membr. Sci.*, 2022, **641**, 119928.

32 Y. Ying, Z. Zhang, S. B. Peh, A. Karmakar, Y. Cheng, J. Zhang, L. Xi, C. Boothroyd, Y. M. Lam, C. Zhong and D. Zhao, *Angew. Chem., Int. Ed.*, 2021, **60**, 11318–11325.

33 A. Matsuoka, S. Nishimori, T. Takahashi, E. Kamio, T. Yoshioka, K. Nakagawa and H. Matsuyama, *Desalination*, 2022, **540**, 115991.

34 E. R. Moore and N. A. Lefevre, *U.S. Patent* 4623678, 1986.

35 S. Lindskog, *Pharmacol. Ther.*, 1997, **74**, 1–20.

36 D. J. Heldebrant, P. G. Jessop, C. A. Thomas, C. A. Eckert and C. L. Liotta, *J. Org. Chem.*, 2005, **70**, 5335–5338.

37 H. Che, M. Huo, L. Peng, T. Fang, N. Liu, L. Feng, Y. Wei and J. Yuan, *Angew. Chem., Int. Ed.*, 2015, **54**, 8934–8938.

38 L. Dong, W. Fan, X. Tong, H. Zhang, M. Chen and Y. Zhao, *J. Mater. Chem. A*, 2018, **6**, 6785–6791.

39 L. Liang, Y. Dong, H. Wang and X. Meng, *Adv. Fiber Mater.*, 2019, **1**, 222–230.

40 H. Musarurwa and N. T. Tavengwa, *React. Funct. Polym.*, 2022, **175**, 105282.

41 D. Yan, Y. Zhao, S. Zhang, X. Wang and X. Ning, *Chem. Eng. J.*, 2024, **493**, 152679.

42 M. Ramezani, S. N. Ellis, A. Riabtseva, M. F. Cunningham and P. G. Jessop, *ACS Omega*, 2023, **8**, 49259–49269.

43 M. Joafshan, A. Shakeri, S. R. Razavi and H. Salehi, *Sep. Purif. Technol.*, 2022, **282**, 119998.

44 J. Zhang, Y. Liu, J. Guo, Y. Yu, Y. Li and X. Zhang, *React. Funct. Polym.*, 2020, **149**, 104503.

45 X. Tan, X. Tan, X. Li, X. Li, Y. Ren, H. Su and H. Li, *Mater. Lett.*, 2024, **354**, 135415.

46 X. Luo, Z. Wang, M. Yan, J. Xin, Y. Yang, L. Zheng and H. Zhang, *J. Polym. Sci.*, 2024, **62**, 2816–2827.

47 X. Gao, X. Zou, H. Ma, S. Meng and G. Zhu, *Adv. Mater.*, 2014, **26**, 3644–3648.

48 X. Ye, J. Zhou, C. Zhang and Y. Wang, *J. Membr. Sci.*, 2022, **662**, 121022.

49 Y. Wang, S. Yang, J. Zhang, Z. Chen, B. Zhu, J. Li, S. Liang, Y. Bai, J. Xu, D. Rao, L. Dong, C. Zhang and X. Yang, *Nat. Commun.*, 2023, **14**, 1108.

50 L. Dong, W. Fan, H. Zhang, M. Chen and Y. Zhao, *Chem. Commun.*, 2017, **53**, 9574–9577.

51 T. F. Dehkordi, A. R. Shirin-Abadi, K. Karimipour and A. R. Mahdavian, *Polymer*, 2021, **212**, 123250.

52 Z. Qi, Y. Liu, Q. Gao, D. Tao, Y. Wang, J. Guo and Y. Yu, *React. Funct. Polym.*, 2023, **182**, 105481.

53 Y. Wang, Y. Shang, X. Li, T. Tian, L. Gao and L. Jiang, *Polymers*, 2014, **6**, 1403–1413.

54 M. Maqsood, M. I. Khan, K. Shaker, M. Umair and Y. Nawab, *J. Text. Inst.*, 2017, **108**, 84–88.

55 Y. Wang, L. F. Villalobos, L. Liang, B. Zhu, J. Li, C. Chen, Y. Bai, C. Zhang, L. Dong, Q. F. An, H. Meng, Y. Zhao and M. Elimelech, *Sci. Adv.*, 2024, **10**, eadn3289.

56 H. Liu, Y. Wang, B. Zhu, H. Li, L. Liang, J. Li, D. Rao, Q. Yan, Y. Bai, C. Zhang, L. Dong, H. Meng and Y. Zhao, *Adv. Mater.*, 2024, **36**, 2311013.

57 P. G. Jessop, S. M. Mercer and D. J. Heldebrant, *Energy Environ. Sci.*, 2012, **5**, 7240–7253.

58 X. Su, P. G. Jessop and M. F. Cunningham, *Macromolecules*, 2012, **45**, 666–670.

59 Y. Liu, P. G. Jessop, M. Cunningham, C. A. Eckert and C. L. Liotta, *Science*, 2006, **313**, 958–960.

60 Y. H. Wang, Z. Y. Cao, Q. H. Li, G. Q. Lin, J. Zhou and P. Tian, *Angew. Chem., Int. Ed.*, 2020, **59**, 8004–8014.

61 Y. Ding, Y. Zhao, X. Wen, Y. Liu, M. Feng and Z. Rui, *Gels*, 2023, **9**, 936.

62 J. Y. Quek, P. J. Roth, R. A. Evans, T. P. Davis and A. B. Lowe, *J. Polym. Sci., Part A: Polym. Chem.*, 2013, **51**, 394–404.

63 M. Z. Griffiths, I. Alkorta and P. L. A. Popelier, *Mol. Inf.*, 2013, **32**, 363–376.

64 D. J. Heldebrant, C. R. Yonker, P. G. Jessop and L. Phan, *Energy Environ. Sci.*, 2008, **1**, 487–493.

65 P. Schattling, I. Pollmann and P. Theato, *React. Funct. Polym.*, 2014, **75**, 16–21.

66 S. Lin, P. Schattling and P. Theato, *Sci. Adv. Mater.*, 2015, **7**, 948–955.

67 M. Nie, X. Li, H. Guo, B. Lei, H. Sun, X. Han and H. Liu, *J. Dispersion Sci. Technol.*, 2018, **39**, 952–960.

68 M. Tanokura, *Biochim. Biophys. Acta, Protein Struct. Mol. Enzymol.*, 1983, **742**, 576–585.

69 M. Chai, Z. Zheng, L. Bao and W. Qiao, *J. Surfactants Deterg.*, 2014, **17**, 383–390.

70 S. Das, S. Sinha, G. Roymahapatra, G. C. De and S. Giri, *J. Phys. Org. Chem.*, 2023, **36**, e4331.

71 Y. N. Hsiao, F. B. Ilhami and C. C. Cheng, *Biomacromolecules*, 2024, **25**, 997–1008.

72 N. B. Darwish, A. Alalawi and N. Alotaibi, *Arabian J. Sci. Eng.*, 2024, **49**, 8049–8055.

73 A. A. Farman, M. Irfan, N. U. Amin, Z. Jahan, X. Song, H. Jiang and S. Gul, *Korean J. Chem. Eng.*, 2022, **39**, 3102–3108.

74 R. Wang, M. Zhang, Y. Guan, M. Chen and Y. Zhang, *Soft Matter*, 2019, **15**, 6107–6115.

75 Y. Wu, Q. Liu, D. Liu, X. P. Cao, B. Yuan and M. Zhao, *Fuel*, 2023, **332**, 126047.

76 Y. Gu, G. Wang, X. Chen, X. Xu, Y. Liu, J. Yang and D. Zhang, *Small*, 2024, **20**, 2402529.

77 T. Xie, H. Zhang, Y. Bai, K. Mei, Y. Zheng, C. Zhang and X. Cheng, *Constr. Build. Mater.*, 2024, **435**, 136651.

78 M. Joafshan, A. Shakeri, S. R. Razavi and H. Salehi, *Sep. Purif. Technol.*, 2022, **282**, 119998.

79 X. Deng, X. Zhou, M. S. Kamal, S. M. S. Hussain, M. Mahmoud and S. Patil, *Molecules*, 2022, **27**, 1195.

80 T. Ni, Y. You, Z. Xie, L. Kong, B. Newman, L. Henderson and S. Zhao, *J. Membr. Sci.*, 2022, **653**, 120543.

81 J. Xu, D. Zhou, J. Ni, B. Li and J. Lian, *Lubr. Sci.*, 2023, **35**, 317–326.

82 W. H. Zhang, M. J. Yin, Q. Zhao, C. G. Jin, N. Wang, S. Ji, C. L. Ritt, M. Elimelech and Q. F. An, *Nat. Nanotechnol.*, 2021, **16**, 337–343.

83 L. Li, Y. Wang, W. Zhang, S. Yu, X. Wang and N. Gao, *Chem. Eng. J.*, 2020, **381**, 122676.

84 H. Liu, L. Liang, F. Tian, X. Xi, Y. Zhang, P. Zhang, X. Cao, Y. Bai, C. Zhang and L. Dong, *Angew. Chem.*, 2024, **136**, e202402509.

85 A. Magazzù and C. Marcuello, *Nanomaterials*, 2023, **13**, 963.

86 S. Li, F. Qin, P. Qin, M. N. Karim and T. Tan, *Green Chem.*, 2013, **15**, 2180–2190.

87 N. D. N. Affandi, Y. B. Truong, I. L. Kyratzis, R. Padhye and L. Arnold, *J. Mater. Sci.*, 2010, **45**, 1411–1418.

88 C. Yin, L. Dong, Z. Wang, M. Chen, Y. Wang and Y. Zhao, *J. Membr. Sci.*, 2019, **592**, 117374.

89 M. Ramezanpour and A. R. Shirin-Abadi, *J. Polym. Res.*, 2021, **28**, 256.

90 H. Kim and T. S. Lee, *Mol. Cryst. Liq. Cryst.*, 2019, **685**, 78–86.

91 K. Wang, Z. Wang, M. Si, X. Liu, G. Liu and Y. Zeng, *Polym. Chem.*, 2024, **15**, 2780–2789.

92 Y. Zhang, L. Liu, X. Liu and Y. Fang, *Langmuir*, 2018, **34**, 2302–2311.

93 A. D. M. Medeiros, C. J. G. D. Silva Junior, J. D. P. D. Amorim, I. J. B. Durval, A. F. D. S. Costa and L. A. Sarubbo, *Processes*, 2022, **10**, 743.

94 Y. Liu, H. He, T. J. Zhang, T. C. Zhang, Y. Wang and S. Yuan, *J. Hazard. Mater.*, 2023, **451**, 131142.

95 L. Hu, S. Gao, X. Ding, D. Wang, J. Jiang, J. Jin and L. Jiang, *ACS Nano*, 2015, **9**, 4835–4842.

96 Y. Cai, D. Chen, N. Li, Q. Xu, H. Li, J. He and J. Lu, *Sci. China: Technol. Sci.*, 2021, **64**, 2211–2219.

97 S. Lin, J. Shang and P. Theato, *ACS Macro Lett.*, 2018, **7**, 431–436.

98 Y. Sun, Y. Liu, X. Zhang, W. Zhang, X. Wang, Y. Yue, J. Guo and Y. Yu, *Sep. Purif. Technol.*, 2021, **279**, 119680.

99 K. M. Shah, I. H. Billinge, X. Chen, H. Fan, Y. Huang, R. K. Winton and N. Y. Yip, *Desalination*, 2022, **538**, 115827.

100 A. Panagopoulos, *Environ. Sci. Pollut. Res.*, 2021, **28**, 21009–21022.

101 B. A. K. Al-Sakaji, S. Al-Asheh and M. A. Maraqa, *Polymers*, 2022, **14**, 2710.

102 W. Suwaileha, D. Johnsona, D. Jonesb and N. Hilal, *Desalination*, 2019, **471**, 114126.

103 U. G. Thummarr, A. Koradiya, M. Saxena, V. Polisetti, P. Ray and P. S. Singh, *Desalination*, 2022, **530**, 115650.

104 P. S. Singh, P. Ray, P. Kallem, S. Maurya and G. S. Trivedi, *Desalination*, 2012, **288**, 8–15.

105 L. Gan, J. Zhang, Y. Wu, Z. Chen, Z. Zhao, S. Lin and Y. Jiang, *Environ. Sci. Technol.*, 2025, **59**, 913–923.

106 A. R. Esfahani, C. Ma, U. A. Flewellen, S. Nair and T. A. L. Harris, *J. Membr. Sci.*, 2023, **678**, 121669.

107 E. Pantuso, E. Ahmed, E. Fontananova, A. Brunetti, I. Tahir, D. P. Karothu, N. A. Alnaji, G. Dushaq, M. Rasras, P. Naumov and G. Di Profio, *Nat. Commun.*, 2023, **14**, 5751.

108 Z. F. Wei, X. Han, C. D. Nie, H. Yang and Y. J. Fu, *Microchem. J.*, 2025, **210**, 112959.

109 A. Vetere, *Fluid Phase Equilib.*, 1997, **132**, 77–91.

110 R. Bhattacherjee, K. Botchway, J. C. Pashin, G. Chakraborty and P. Bikkina, *Fuel*, 2024, **368**, 131577.

111 C. Kim and B. Lee, *J. Environ. Chem. Eng.*, 2024, **12**, 113399.

112 K. Sato, K. Sugimoto and T. Nakane, *J. Membr. Sci.*, 2008, **319**, 244–255.

113 J. Hu, M. Li, L. Wang and X. Zhang, *J. Membr. Sci.*, 2021, **618**, 118698.

114 M. Li, K. Li, L. Wang and X. Zhang, *Water Res.*, 2020, **172**, 115488.

115 Y. Lu, D. Sun, J. Ralston, Q. Liu and Z. Xu, *J. Colloid Interface Sci.*, 2019, **557**, 185–195.

116 L. Liu, C. Zheng and H. Lu, *J. Dispersion Sci. Technol.*, 2017, **38**, 1824–1831.